Supporting Information

Molecular Configuration-Controlled Copper(I)-Halide Cluster Achieving Near-Unity Emission Efficiency for Green and Green-Sensitized Blue Electroluminescence

Xiao Li[1, 3], Sai Guo[1, 3], Xin Liu[1, 3], Yu-Fu Sun[1, 3], Dong-Hai Zhang[1, 3], Hui Yang[1, 3], Jia-Min Lu[2*] & Xu-Lin Chen[1, 3*]

[1] State Key Laboratory of Structural Chemistry, Fujian Institute of Research on the Structure of Matter, Chinese Academy of Sciences, Fuzhou, 350002, Fujian

[2] Clinical Research Institute, the First Affiliated Hospital of Xiamen University, School of Medicine Xiamen University, Xiamen, 361003, Fujian

[3] Xiamen Key Laboratory of Rare Earth Photoelectric Functional Materials, Xiamen Institute of Rare Earth Materials, Chinese Academy of Sciences, Xiamen, 361021, Fujian

*Corresponding Authors: xlchem@fjirsm.ac.cn; lujiamin@xmu.edu.cn

Contents

General Information

All air and moisture sensitive reactions were carried out in an argon atmosphere. The solvents and reactants were purchased from commercial sources and used without further purification except as noted. The prepared copper(I) clusters were twice dried and recrystallized before device fabrication. ^{1}H NMR, ^{31}P and ^{13}C NMR were obtained using a Bruker Avance III nuclear magnetic resonance spectrometer at a frequency of 500 Hz in deuterated chloroform ($CDCl_3$). Thermogravimetric analysis (TGA) was performed by TGA in a nitrogen atmosphere at a heating rate of 10 K/min. Single crystal X-ray diffraction data were collected on a Bruker-D8 VENTRUE diffractometer with an X-ray source of Mo kα. Cyclic voltammetry was performed with a scan rate of 100 mV/s at room temperature in anhydrous and argon-saturated dichloromethane solutions of 0.1 M tetrabutylammonium hexafluorophosphate and 1.0 mM investigated cluster with a CHI840D electrochemical analyzer. Glassy carbon, platinum wire and Ag/Ag^{+} (0.01 M of $AgNO_3$ in acetonitrile) were selected as the working electrode, auxiliary electrode and reference electrode, respectively. The ferrocenium/ferrocene couple was used as an internal standard. The UV-VIS absorption spectra were recorded by Agilent Cary 5000 UV-VIS spectrophotometer under ambient conditions. The absolute photoluminescence quantum yields (PLQYs) were measured under a nitrogen atmosphere using an integrating sphere coupled with a photoluminescence measurement unit (Quantaurus-QY, C11347-11). Steady-state photoluminescence (PL) spectra were recorded on an Edinburgh FLS980 spectrometer using a xenon lamp as the excitation source. Transient PL decay curves were measured on the same instrument in multi-channel scaling (MCS) mode, using an NT242-1K OPO laser as the excitation source.

Synthesis Method

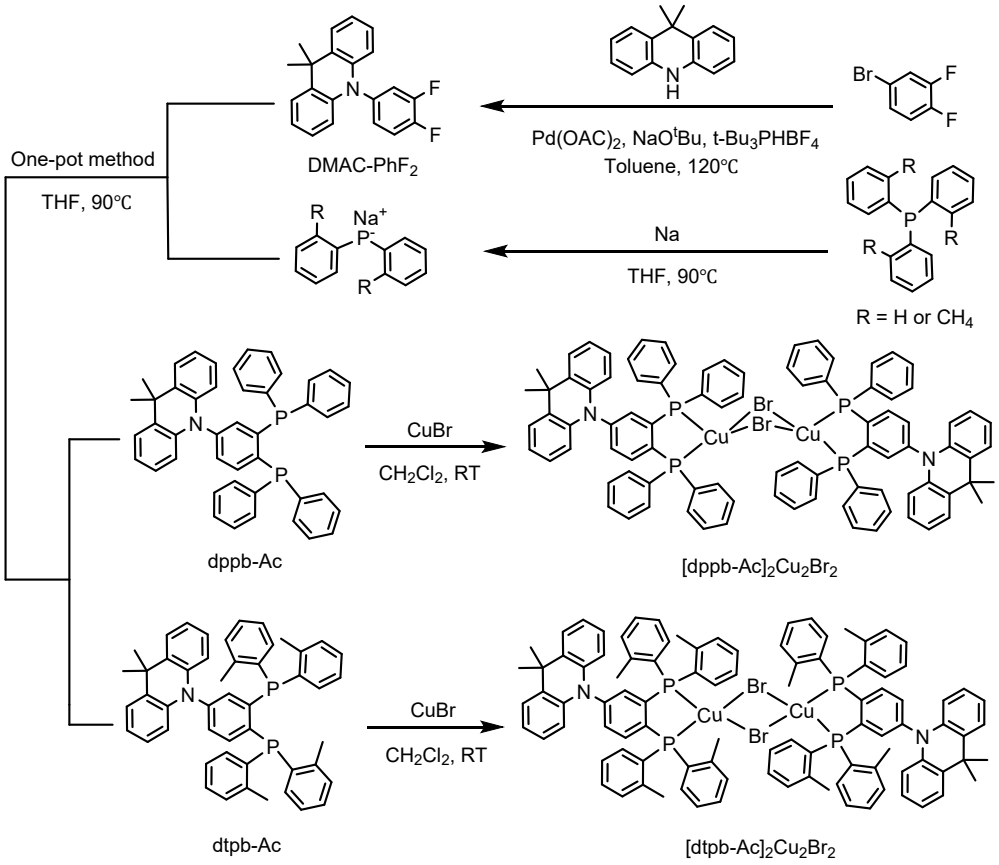

Figure S1. Synthetic route of $[dppb\text{-}Ac]_2Cu_2Br_2$ and $[dtpb\text{-}Ac]_2Cu_2Br_2$.

DMAC-PhF_2[1]: In a 500 ml three-neck flask, 3.86 g (20 nmol) of 4-bromo-1,2-difluorobenzene, 4.19 g (20 nmol) of 9,10-dihydro-9,9-dimethylacridine, 1.92 g (20 nmol) of sodium tert-butoxide, 0.29 g (1 nmol) of tri-tert-butylphosphonium tetrafluoroborate, 0.55 g (0.6 nmol) of tris(dibasic benzylacetone) dipalladium, with 100 ml of dry toluene as solvent, and stirred at reflux for 12 h at 120°C under argon atmosphere. The extracted organics were washed with ethyl acetate and saturated saline and dried by adding $MgSO_4$. The desiccant was removed by filtration and the solvent was removed under vacuum to give a gray-brown solid. The residue was purified by chromatography on silica gel (petroleum ether/dichloromethane, 5:1) to give 5.52 g (86%) of white solid. ^{1}H NMR (500 MHz, Chloroform-*d*) δ 7.53 (dd, *J* = 7.6, 1.7 Hz, 2H), 7.51 – 7.44 (m, 1H), 7.29 – 7.24 (m, 1H), 7.17 (ddt, *J* = 8.3, 3.9, 2.0 Hz, 1H), 7.07 (td, *J* = 7.7, 1.7 Hz, 2H), 7.02 (td, *J* = 7.4, 1.4 Hz, 2H), 6.33 (dd, *J* = 8.1, 1.4 Hz, 2H), 1.75 (s, 6H).

dppb-Ac²: In a 200 ml round bottom flask, 4.72 g (18 nmol) of triphenylphosphine, 1.86 g (81 nmol) of sodium, with 50 ml of anhydrous tetrahydrofuran as a solvent, were stirred under reflux under argon atmosphere for 12 h. The cooled crimson solution was transferred to another dry 200 ml round bottom flask containing 1.93 g (6 nmol) of DMAC-PhF_2 in a refluxed under argon atmosphere for three hours and then stirred at room temperature for three hours. After completion of the reaction, an appropriate amount of methanol was added to the solution. The extracted organics were washed with ethyl acetate and saturated saline and dried by adding $MgSO_4$. The desiccant was removed by filtration and the solvent was removed in vacuum to give a yellowish brown solid. The residue was purified by chromatography on silica gel (petroleum ether/dichloromethane, 4:1) to give 1.96 g (50%) of white solid. ^{1}H NMR (500 MHz, Chloroform-*d*) δ 7.45 (dd, *J* = 7.8, 1.6 Hz, 2H), 7.33 (q, *J* = 2.5 Hz, 10H), 7.30 – 7.18 (m, 14H), 7.03 (td, *J* = 7.7, 1.6 Hz, 2H), 6.96 (td, *J* = 7.4, 1.3 Hz, 2H), 6.30 (dd, *J* = 8.2, 1.2 Hz, 2H), 1.63 (s, 6H). ^{13}C NMR (126 MHz, Chloroform-*d*) δ 146.70, 146.61, 146.48, 146.39, 144.23, 144.16, 144.00, 143.94, 141.93, 140.78, 137.15, 137.11, 136.79, 136.75, 136.71, 136.67, 136.59, 136.55, 136.51, 136.47, 136.30, 136.24, 134.23, 134.21, 134.09, 134.07, 133.72, 133.71, 133.58, 133.56, 131.61, 130.50, 128.73, 128.54, 128.50, 128.43, 128.38, 126.31, 124.94, 120.84, 114.15, 36.00, 30.43.

dtpb-Ac²: In a 200 ml round bottom flask, 5.48 g (18 nmol) of tris(2-methylphenyl)phosphine, 0.14 g (0.98 nmol) of 1-methylnaphthalene, and 1.86 g (81 nmol) of sodium were stirred by refluxing 50 ml of anhydrous tetrahydrofuran as a solvent for 12 h in an atmosphere of argon, and the cooled crimson colored solution was transferred to another dry one containing 1.93 g (6 nmol) of DMAC-PhF_2 to another dry 200 ml round-bottomed flask containing 1.93 g (6 nmol) of DMAC-PhF_2 was refluxed under argon atmosphere for three hours and then stirred at room temperature for three hours. After completion of the reaction, an appropriate amount of methanol was added to the solution. The extracted organics were washed with ethyl acetate and saturated saline and dried by adding $MgSO_4$. The desiccant was removed by filtration and the solvent was removed in vacuum to give a yellowish

brown solid. The residue was purified by chromatography on silica gel (petroleum ether/dichloromethane, 4:1) to give 1.62 g (38%) of white solid. ^{1}H NMR (500 MHz, Chloroform-*d*) δ 7.42 (dd, *J* = 7.7, 1.6 Hz, 2H), 7.27 – 7.20 (m, 7H), 7.17 – 7.07 (m, 8H), 7.04 – 6.93 (m, 9H), 6.88 (dd, *J* = 7.8, 2.2 Hz, 3H), 6.80 (d, *J* = 5.7 Hz, 2H), 6.29 (dd, *J* = 8.2, 1.3 Hz, 2H), 2.30 (d, *J* = 15.5 Hz, 12H), 1.60 (s, 6H). ^{13}C NMR (126 MHz, Chloroform-*d*) δ 141.95, 140.73, 133.56, 131.67, 130.34, 130.07, 128.61, 128.58, 126.28, 125.94, 125.05, 120.69, 113.91, 35.94, 30.67, 21.22, 21.07, 1.04.

[dppb-Ac]$_2$Cu$_2$Br$_2$: (72 mg, 0.50 mmol) copper bromide was added to a solution of CH_2Cl_2 (5 ml) containing (0.33 g, 0.50 mmol) of dppb-Ac. The mixture was stirred at room temperature for 3 h. The reaction mixture was filtered and the solvent was removed in vacuo to give a yellow powder. The residue was purified by recrystallization with CH_2Cl_2/ether to give 295 mg of yellow crystals. 74% yield.^{1}H NMR (500 MHz, Chloroform-*d*) δ 7.42 – 7.29 (m, 22H), 7.26 – 7.13 (m, 11H), 7.12 (t, *J* = 7.3 Hz, 12H), 7.04 (t, *J* = 7.5 Hz, 8H), 6.99 – 6.96 (m, 4H), 6.94 – 6.91 (m, 4H), 6.14 (d, *J* = 9.4 Hz, 4H), 1.59 (s, 12H). ^{13}C NMR (126 MHz, $CDCl_3$) δ 147.02, 146.78, 146.54, 142.82, 142.57, 142.55, 142.34, 140.57, 136.63, 136.58, 136.52, 136.48, 134.03, 134.00, 133.93, 133.90, 133.83, 133.80, 132.66, 132.57, 132.51, 132.42, 132.33, 132.24, 132.18, 132.09, 131.95, 131.93, 130.46, 129.25, 128.32, 128.30, 128.24, 128.18, 128.16, 126.44, 125.10, 121.02, 114.13, 77.36, 77.10, 76.85, 36.00, 30.65. ^{31}P NMR (202 MHz, Chloroform-*d*) δ -20.68. Elemental Analysis. calcd for [dppb-Ac]$_2$Cu$_2$Br$_2$: C 67.80%, H 4.68%, N 1.76%. Found: C 67.75%, H 4.74%, N 1.74%.

[dtpb-Ac]$_2$Cu$_2$Br$_2$: (72 mg,0.50 mmol) of copper bromide was added to a solution of CH_2Cl_2 (5 ml) containing (0.36 g,0.50 mmol) of dtpb-Ac. The mixture was stirred at room temperature for 3 h. The reaction mixture was filtered and the solvent was removed in vacuo to give a green powder. The residue was purified by recrystallization with CH_2Cl_2 /ether to give 213 mg of green crystals. 50% yield.^{1}H NMR (500 MHz, Chloroform-d) δ 7.51 – 7.43 (m, 8H), 7.31 (t, J = 5.3 Hz, 4H), 7.28 – 7.05 (m, 16H), 7.05 – 6.87 (m, 16H), 6.73 (d, J = 8.7 Hz, 6H), 6.28 (dd, J = 7.7, 1.7 Hz, 4H), 2.60 (d, J = 20.9

Hz, 24H), 1.61 (s, 12H). ^{13}C NMR (126 MHz, Chloroform-*d*) δ 144.22, 144.20, 143.96, 143.71, 142.62, 140.36, 138.92, 137.31, 136.01, 135.98, 135.94, 132.00, 131.98, 131.29, 130.44, 126.36, 126.19, 125.27, 121.73, 114.78, 36.20, 30.31, 22.92, 22.85, 22.82, 22.78, 22.76, 22.72. ^{31}P NMR (202 MHz, Chloroform-*d*) δ -26.49. Elemental Analysis. calcd for $[dtpb\text{-}Ac]_2Cu_2Br_2$: C 68.97%, H 5.32%, N 1.64%. Found: $[dtpb\text{-}Ac]_2Cu_2Br_2$: C 69.28%, H 5.38%, N 1.62%.

Crystal Structures

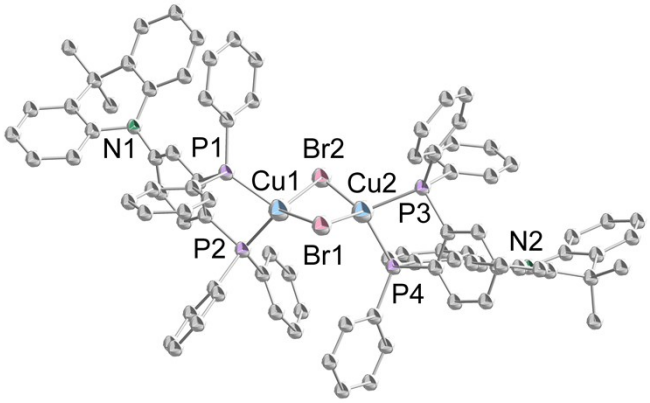

Figure S2. Crystal structure of $[dppb\text{-}Ac]_2Cu_2Br_2$.

Table S1. Crystal parameters and refinement data of $[dppb\text{-}Ac]_2Cu_2Br_2$.

Compounds	$[dppb\text{-}Ac]_2Cu_2Br_2$
Empirical formula	$C_{90}H_{74}Br_2Cu_2N_2P_4$
Formula weight	1594.29
Temperature/K	200
Crystal system	triclinic
Space group	P-1
a/Å	14.690(5)
b/Å	15.389(5)
c/Å	18.808(6)
α/°	89.860(13)
β/°	80.343(12)
γ/°	77.503(13)
Volume/Å^3	4090(2)
Z	2
ρcalcg/cm^3	1.295
μ/mm^{-1}	1.62
F(000)	1632
Crystal size/mm^3	0.02 × 0.01 × 0.003

Radiation	MoKα (λ = 0.71073)
2Θ range for data collection/°	4.338 to 49.264
Index ranges	-17 ≤ h ≤ 17, -17 ≤ k ≤ 17, -21 ≤ l ≤ 21
Reflections collected	131991
Independent reflections	13656 [R_{int} = 0.0956, R_{sigma} = 0.0410]
Data/restraints/parameters	13656/0/914
Goodness-of-fit on F^2	1.025
Final R indexes [I>=2σ (I)]	R_1 = 0.0390, wR_2 = 0.0879
Final R indexes [all data]	R_1 = 0.0571, wR_2 = 0.0965
Largest diff. peak/hole / e $Å^{-3}$	0.52/-0.53

Table S2. Selected bond length (Å) and bond angles (deg) of $[dppb\text{-}Ac]_2Cu_2Br_2$.

Cu1-Br1	2.5470(10)
Cu1-Br2	2.4178(10)
Cu1-Cu2	2.8517(10)
Cu2-P3	2.2777(11)
Cu2-P4	2.2705(12)
Br1-Cu2	2.4378(10)
Br2-Cu2	2.5158(10)
P1-Cu1	2.2580(10)
P2-Cu1	2.2683(11)
Cu1-Br1-Cu2	69.75(2)
Cu1-Br2-Cu2	70.59(2)
Br1-Cu2-Br2	107.74(2)
Br1-Cu2-P3	119.78(3)
Br2-Cu2-P4	110.74(3)
Br1-Cu1-Br2	107.37(2)
P3-Cu2-P4	87.14(4)
P1-Cu1-P2	89.18(4)
P1-Cu1-Br1	108.39(3)
P2-Cu1-Br2	130.34(3)

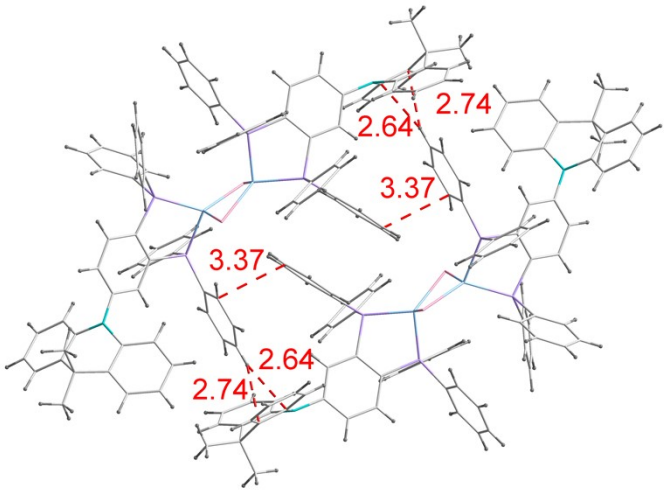

Figure S3. Single-crystal packing diagram of $[dppb\text{-}Ac]_2Cu_2Br_2$.

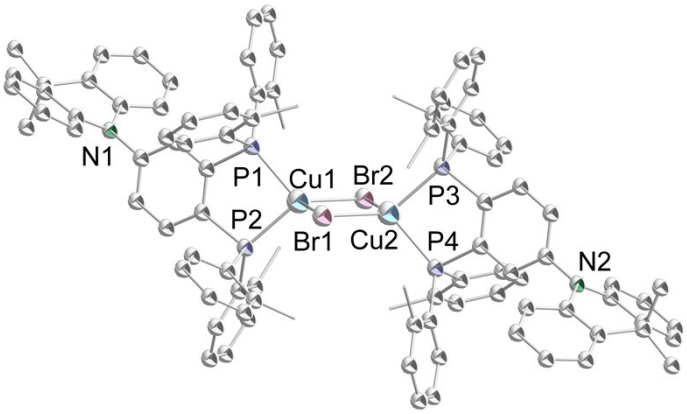

Figure S4. Crystal structure of $[dtpb\text{-}Ac]_2Cu_2Br_2$.

Table S3. Crystal parameters and refinement data of $[dtpb\text{-}Ac]_2Cu_2Br_2$.

Compounds	$[dtpb\text{-}Ac]_2Cu_2Br_2$
Empirical formula	$C_{98}H_{90}Br_2Cu_2N_2P_4$
Formula weight	1706.49
Temperature/K	200
Crystal system	triclinic
Space group	P-1
a/Å	11.0201(7)
b/Å	13.1886(8)
c/Å	15.3030(10)
α/°	100.628(3)
β/°	90.218(3)
γ/°	106.976(3)
Volume/Å^3	2086.8(2)
Z	1

ρcalcg/cm^3	1.358
μ/mm^{-1}	1.592
F(000)	880
Crystal size/mm^3	0.201 × 0.102 × 0.1
Radiation	MoKα (λ = 0.71073)
2Θ range for data collection/°	3.872 to 53.62
Index ranges	-13 ≤ h ≤ 13, -16 ≤ k ≤ 16, -19 ≤ l ≤ 19
Reflections collected	41104
Independent reflections	8906 [R_{int} = 0.1061, R_{sigma} = 0.0890]
Data/restraints/parameters	8906/0/493
Goodness-of-fit on F^2	1.015
Final R indexes [I>=2σ (I)]	R_1 = 0.0557, wR_2 = 0.1099
Final R indexes [all data]	R_1 = 0.1270, wR_2 = 0.1388
Largest diff. peak/hole / e Å^{-3}	0.79/-0.46

Table S4. Selected bond length (Å) and bond angles (deg) of $[dtpb\text{-}Ac]_2Cu_2Br_2$.

Cu1-Br1	2.4938(7)
Cu1-Br2	2.4226(8)
Cu2-P2	2.2881(12)
Cu2-P4	2.2775(14)
Br1-Cu2	2.4226(8)
Br2-Cu2	2.4938(7)
P1-Cu1	2.2775(14)
P3-Cu1	2.2881(12)
Cu1-Br2-Cu2	78.23(2)
Cu1-Br1-Cu2	78.23(2)
Br1-Cu1-Br2	101.77(2)
Br1-Cu2-Br2	101.77(2)
Br2-Cu2-P2	108.48(4)
Br1-Cu2-P4	122.12(4)
P1-Cu1-P1B	90.79(4)
P3-Cu1-Br1	108.48(4)
P1-Cu1-Br2	122.12(4)
P2-Cu2-P4	90.79(4)

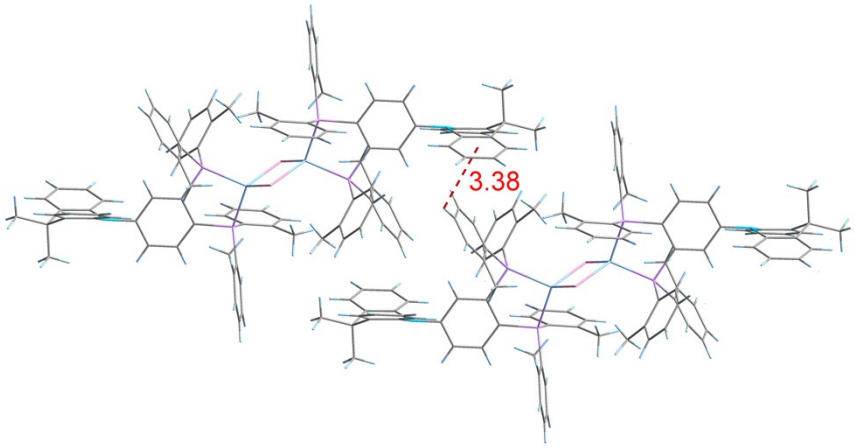

Figure S5. Single-crystal packing diagram of $[dtpb\text{-}Ac]_2Cu_2Br_2$.

Thermogravimetric Analysis

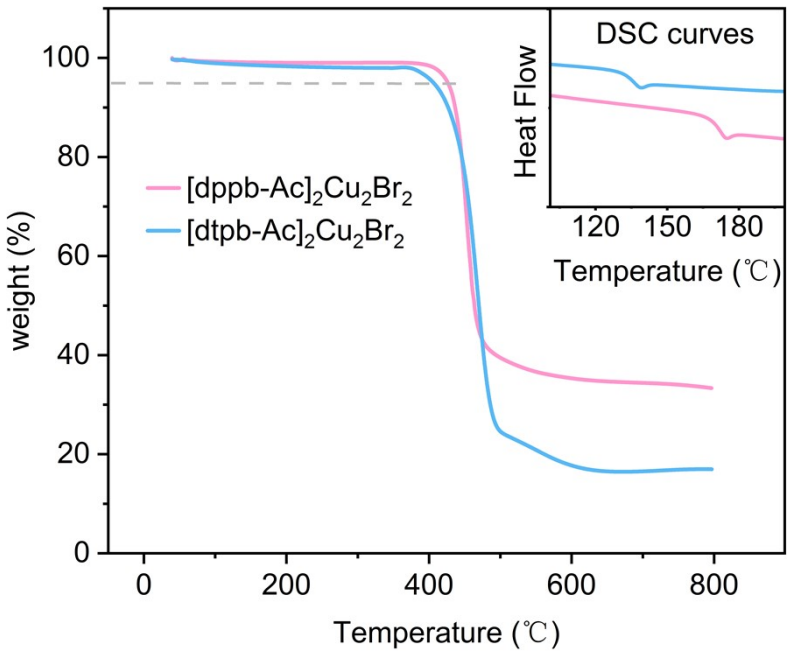

Figure S6. TGA curves and DSC curves of $[dppb\text{-}Ac]_2Cu_2Br_2$ and $[dtpb\text{-}Ac]_2Cu_2Br_2$. The Gray dashed line marks 95% of the original sample weight.

Electrochemical Properties

Cyclic voltammetry was performed at room temperature in anhydrous and argon-saturated dichloromethane solutions of 0.1 M tetrabutylammonium hexafluorophosphate and 1.0 mM investigated compounds with a CHI840D electrochemical analyzer. Glassy carbon, platinum wire and Ag/Ag^+(0.01 M of $AgNO_3$ in acetonitrile) were selected as the working electrode, auxiliary

electrode and reference electrode, respectively. The ferrocenium/ferrocene couple was used as an internal standard. The HOMO and LUMO energy levels were estimated from the cyclic voltammetry and optical bandgaps (E_g) determined from the onset of the absorption band (λ_{onset}).

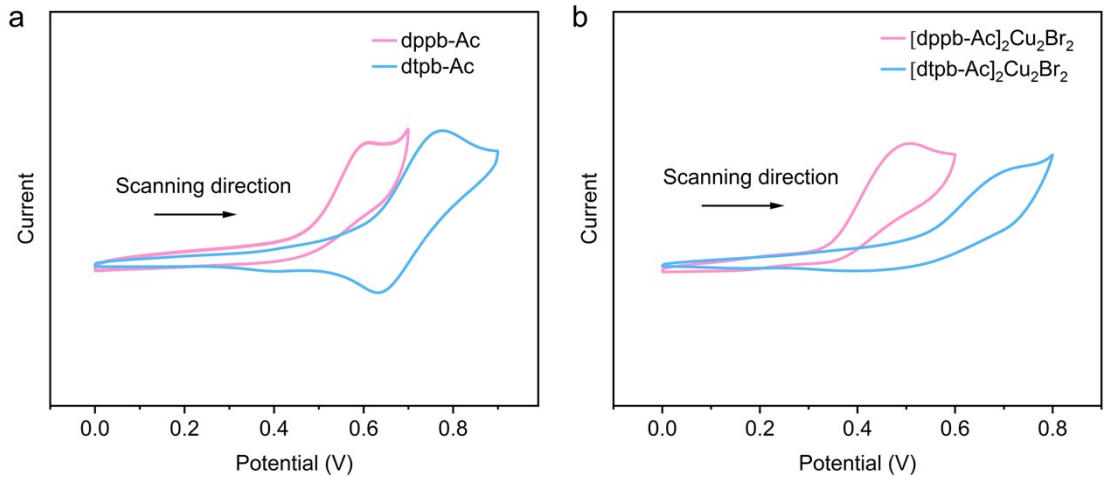

Figure S7. a) Cyclic voltammograms for the oxidation of dppb-Ac and dtpb-Ac in dichloromethane at room temperature; b) Cyclic voltammograms for the oxidation of $[dppb\text{-}Ac]_2Cu_2Br_2$ and $[dtpb\text{-}Ac]_2Cu_2Br_2$ in dichloromethane at room temperature (rate: 100 mV/s, concentration: 1 mM, ferrocenium/ferrocene couple was used as an internal standard).

Table S5. Summary of CV data and energy levels.

Compound	E_{ox} [a)] [ev]	$E_{FC/Fc+}$ [b)] [ev]	E_g [c)] [ev]	E_{HOMO} [d)] [ev]	E_{LUMO} [e)] [ev]
dppb-Ac	0.54	0.20	3.10	-5.14	-2.04
dtpb-Ac	0.67	0.20	3.23	-5.27	-2.04
$[dppb\text{-}Ac]_2Cu_2Br_2$	0.41	0.20	2.80	-5.01	-2.21
$[dtpb\text{-}Ac]_2Cu_2Br_2$	0.59	0.20	2.89	-5.19	-2.30

[a)] the oxidation potentials (E_{OX}) were acquired by using the half-peak potentials determined as described in the literature[3]; [b)] ferrocenium/ferrocene couple was used as an internal standard; [c)] calculated from the absorption edge λ_{onset} using equation: $1241/\lambda_{onset}$; [d)] calculated using the equation: $E_{HOMO} = -[E_{OX} - E_{Fc/Fc+} + 4.8]$ eV; [e)] calculated from E_g and E_{HOMO} using the equation: $E_{LUMO} = (E_{HOMO} + E_g)$ (eV).

Computational Methodology and Results

The density functional theory (DFT) and time-dependent DFT (TD-DFT) calculations were performed with the Gaussian 09 program package 3 The density functional theory (DFT) calculations at the B3LYP/6-31G* level was used to optimize the ground state geometries of the investigated compounds. and the associated basis sets Lanl08 (f) and Lanl08 (d) for Cu and Br. Time-dependent density functional theory (TD-DFT) calculations was performed at the same level using the optimized ground state geometries. The electron density diagrams of molecular orbitals were generated using GaussView program. The partition orbital composition was analyzed with the Multiwfn 2.4 program.[4] The image is generated by using VMB program.[5]

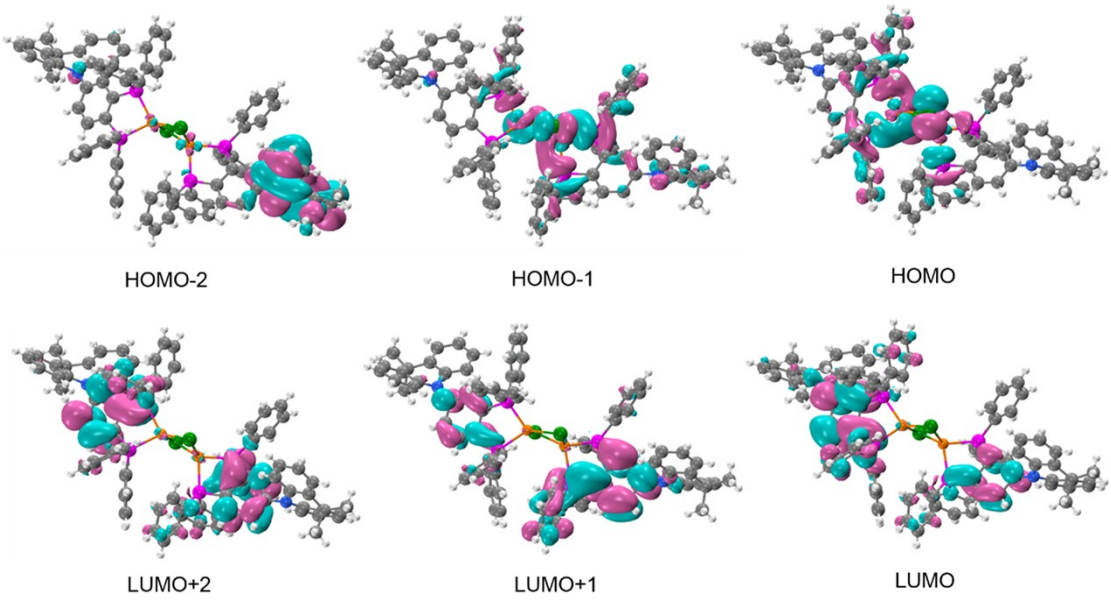

Figure S8. Distributions and energy levels of the first three highest occupied (HOMO~HOMO-2) and lowest unoccupied molecular orbitals (LUMO~LUMO+2) of $[dppb\text{-}Ac]_2Cu_2Br_2$.

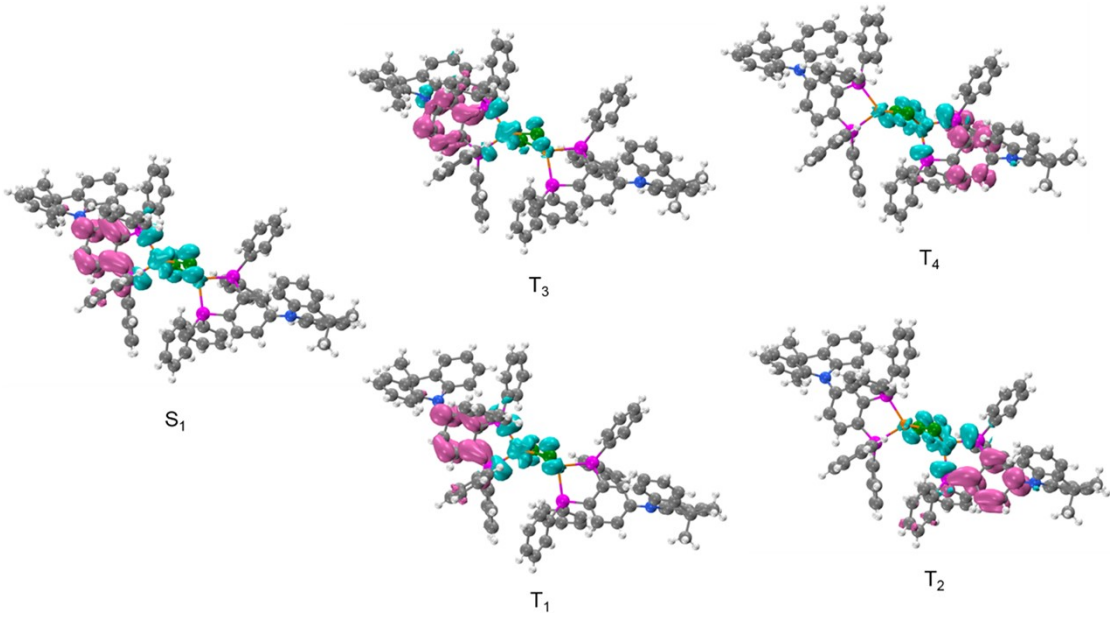

Figure S9. Distributions of the excited states of $[dppb\text{-}Ac]_2Cu_2Br_2$ simulated

Table S6. Composition of the frontier orbitals of $[dppb\text{-}Ac]_2Cu_2Br_2$.

	Cu	Br	dppb-Ac	DMAC	P atom
HOMO	32.75%	22.19%	45.06%	0.65%	44.41%
LUMO	1.09%	0.45%	98.45%	6.87%	91.58%

Table S7. Compositions of hole and electron in the S_1 and T_1 states of $[dppb\text{-}Ac]_2Cu_2Br_2$.

		Cu	Br	dppb-Ac	DMAC	P atom
S_1	hole	33.17%	19.71%	47.12%	1.11%	46.01%
	electron	1.04%	0.30%	98.67%	4.84%	93.83%
	difference	32.14%	19.41%	-51.55%	-3.73%	-47.82%
T_1	hole	33.44%	17.32%	49.24%	1.68%	47.56%
	electron	1.03%	0.29%	98.67%	4.83%	93.84%
	difference	32.41%	17.03%	-49.44%	-3.15%	-46.29%

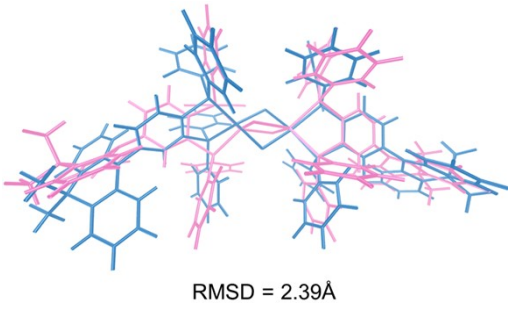

Figure S10. Geometry comparison between S_0(pink) and S_1(blue) states of $[dppb\text{-}Ac]_2Cu_2Br_2$.

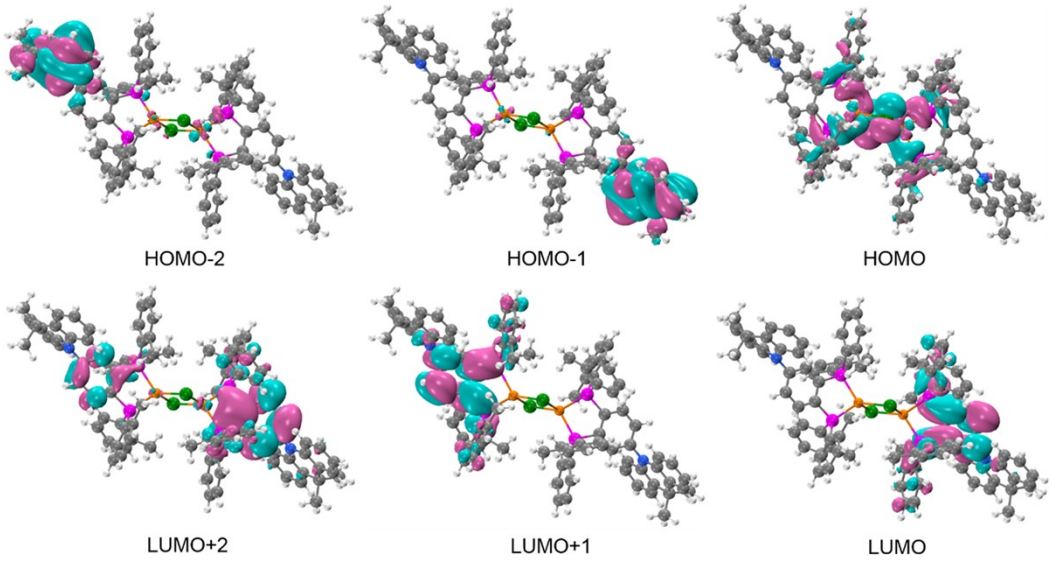

Figure S11. Distributions and energy levels of the first three highest occupied (HOMO~HOMO-2) and lowest unoccupied molecular orbitals (LUMO~LUMO+2) of $[dtpb\text{-}Ac]_2Cu_2Br_2$.

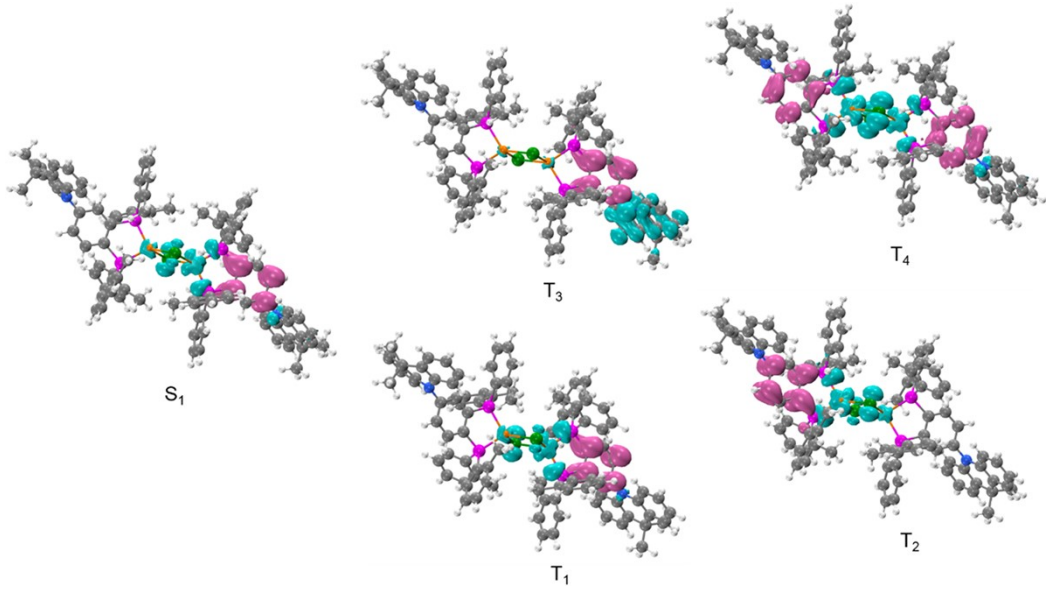

Figure S12. Distributions of the excited states of $[dtpb\text{-}Ac]_2Cu_2Br_2$ simulated.

Table S8. Composition of the frontier orbitals of $[dtpb\text{-}Ac]_2Cu_2Br_2$.

	Cu	Br	dtpb-Ac	DMAC	P atom
HOMO	31.76%	21.07%	47.17%	1.99%	45.18%
LUMO	0.42%	0.08%	99.50%	5.31%	94.19%

Table S9. Compositions of hole and electron in the S_1 and T_1 of $[dtpb\text{-}Ac]_2Cu_2Br_2$.

		Cu	Br	dtpb-Ac	DMAC	P atom
S_1	hole	24.94%	16.68%	58.38%	18.08%	40.30%
	electron	0.40%	0.02%	99.58%	2.68%	96.90%
	difference	24.54%	16.66%	-41.2%	15.40%	-56.60%
T_1	hole	29.40%	18.31%	52.29%	5.50%	46.79%
	electron	0.40%	0.02%	99.58%	2.68%	96.90%
	difference	29.00%	18.29%	-47.29%	2.82%	-50.11%

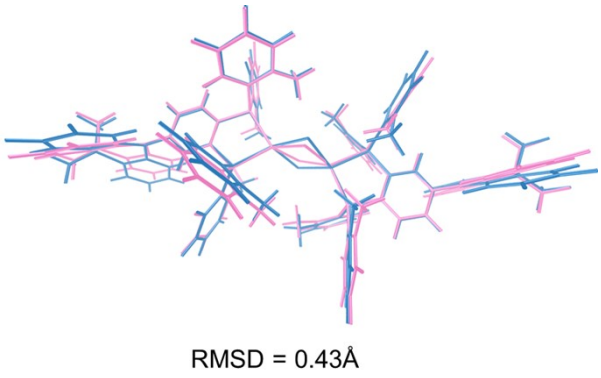

Figure S13. Geometry comparison between S_0(pink) and S_1(blue) states of $[dtpb\text{-}Ac]_2Cu_2Br_2$.

Photophysical Properties

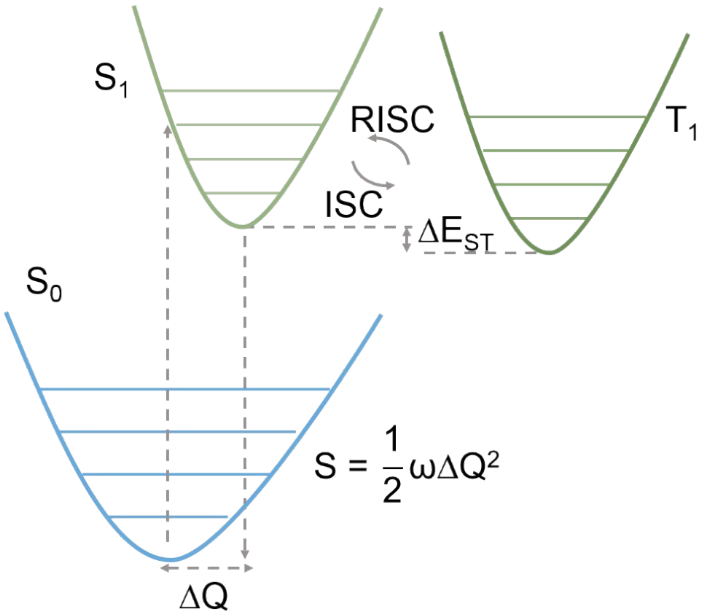

Figure S14. The energy levels of S_0, S_1 and T_1 state and the photophysical processes between the energy levels.

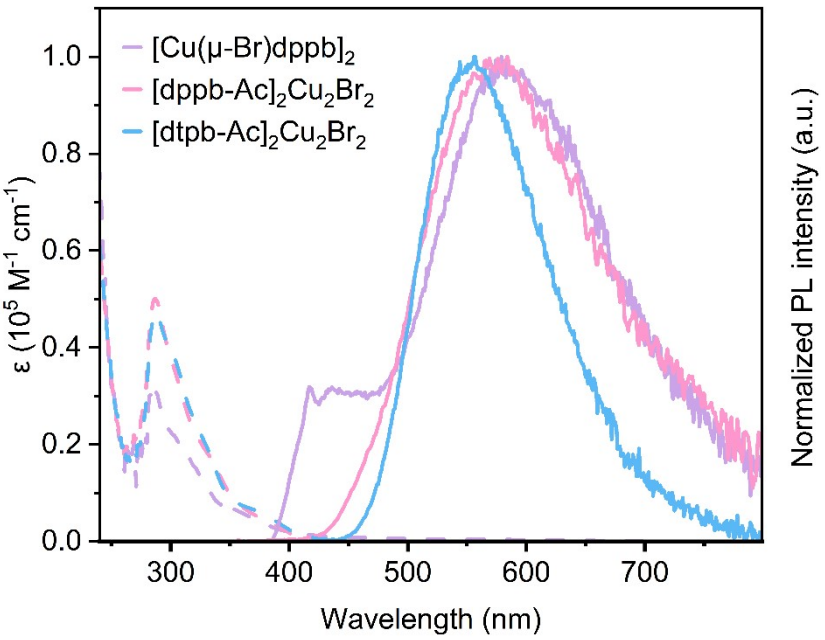

Figure S15. Absorption and PL spectra measured in dichloromethane (c = 1 × 10^{-5} M) at room temperature

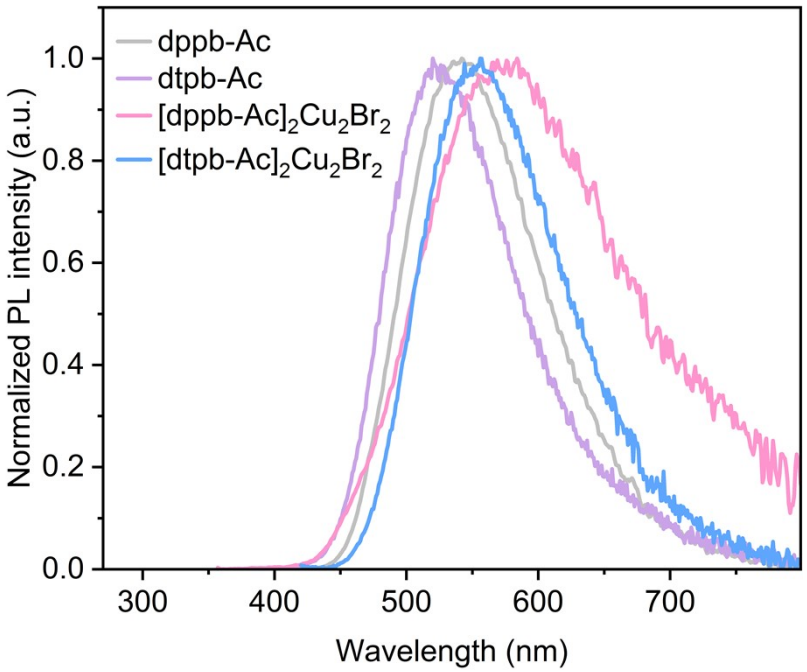

Figure S16. PL spectra measured in dichloromethane (c = 1 × 10^{-5} M) at room temperature.

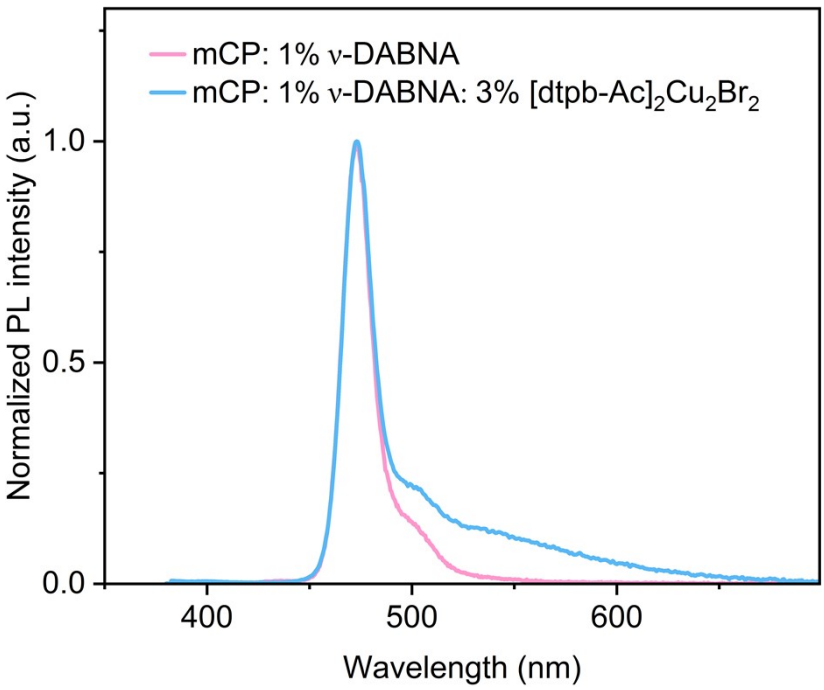

Figure S17. Normalized PL spectra of the unsensitized film (1 wt% *v*-DABNA: mCP) and the sensitized film (1 wt% *v*-DABNA: 3% [dtpb-Ac]$_2$Cu$_2$Br$_2$: mCP).

Energy transfer process in the sensitization system (donor: [dtpb-Ac]2Cu2Br2; acceptor: ν-DABNA) [6]

The Förster radius (R_{FRET}) was calculated according to Equation S1:

$$R_{FRET}^{6} = \frac{9000\ln 10 k^2 \Phi_D}{128\pi^5 N_A n^4} \int_0^\infty F_D(\lambda)\varepsilon_A(\lambda)\lambda^4 d\lambda \quad \text{Equation S1}$$

Here, κ denotes the orientation factor and is taken as $\kappa^2 = 2/3$, assuming a random orientation of transition dipoles between the donor and the acceptor. Φ_D represents the photoluminescence quantum yield of the donor film in the absence of the acceptor. N_A is Avogadro's number, and *n* is the refractive index of the medium. The overlap integral, $\int_0^\infty F_D(\lambda)\varepsilon_A(\lambda)\lambda^4 d\lambda$, describes the spectral overlap between the donor photoluminescence and the acceptor absorption. Here, $F_D(\lambda)$ corresponds to the donor emission spectrum corrected and normalized to unity, while $\varepsilon_A(\lambda)$ denotes the absorption spectrum of the acceptor expressed in terms of the extinction

coefficient (measured in toluene); λ represents the wavelength. Based on these parameters, the calculated R_{FRET} values are 5.79 nm for $[dtpb\text{-}Ac]_2Cu_2Br_2$.

The FRET rates (k_{FRET}) in the EML were evaluated based on the radiative decay rates using the following Equation S2:

$$k_r = \tau_r^{-1} \approx k_D + k_{FRET} \quad \text{Equation S2}$$

In this equation, k_r denotes the radiative decay rate of the sensitized film (1 wt% *v*-DABNA: 3% $[dtpb\text{-}Ac]_2Cu_2Br_2$: mCP, $k_r = 4.85 \times 10^5\ s^{-1}$), whereas k_D refers to the radiative decay rate of the donor in the absence of the acceptor ($1.22 \times 10^5\ s^{-1}$). Using Equation S2, the k_{FRET} value was determined to be $3.63 \times \times 10^5\ s^{-1}$. The FRET efficiency ($\Phi_{FRET}$), defined as the fraction of excitons decaying radiatively via energy transfer to the acceptor, was calculated using Equation S3, yielding values of 74.8% for the sensitized film

$$\Phi_{FRET} = \frac{k_{FRET}}{k_D + k_{FRET}} \quad \text{Equation S3}$$

The donor–acceptor distance R_{DA} was calculated to be 4.84 nm (Equation S4). Given these relatively large distances, it is reasonable to disregard short-range Dexter energy transfer and instead consider long-range FRET as predominant contributor to the excited-state dynamics of the sensitization system.

$$k_{FRET} = \frac{1}{\tau_D}\left(\frac{R_{FRET}}{R_{DA}}\right)^6 \quad \text{Equation S4}$$

Device Fabrication and Characterization

Glass substrates pre-coated with a 120 nm of indium tin oxide (ITO) with a sheet resistance of 15 Ω per square were cleaned in ultrasonic bath of deionized water, acetone, and isopropanol in turn for 15 minutes each. Subsequently, the ITO glass substrates were dried using a stream of Ar gas and irradiated by UV-ozone for 15 minutes. The organic materials were deposited onto the ITO-coated substrates at a rate of 1 Å/s under high vacuum ($< 2\times10^{-5}$) via thermal evaporation in a vacuum

chamber. Following this deposition, a layer of Liq and another layer of Al were sequentially deposited at rates of 0.1 Å/s and 3 Å/s, respectively. The intersection of the ITO and the Al electrodes gave an active device area of 9 mm^2. The EL spectra, CIE coordinates, CEs, PEs, EQEs, and current density-voltage-luminance curves (I-V-L) of the OLEDs were measured by an integrated optoelectronic performance test system including a calibrated spectra radiometer (TOPCON SR-UL1R) and a Keithley 2400 source meter.

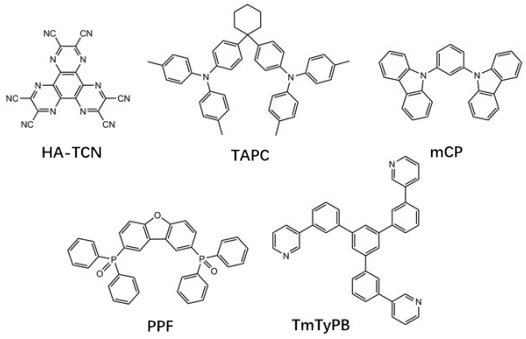

Figure S18. Molecular structures of the functional materials used in the OLEDs.

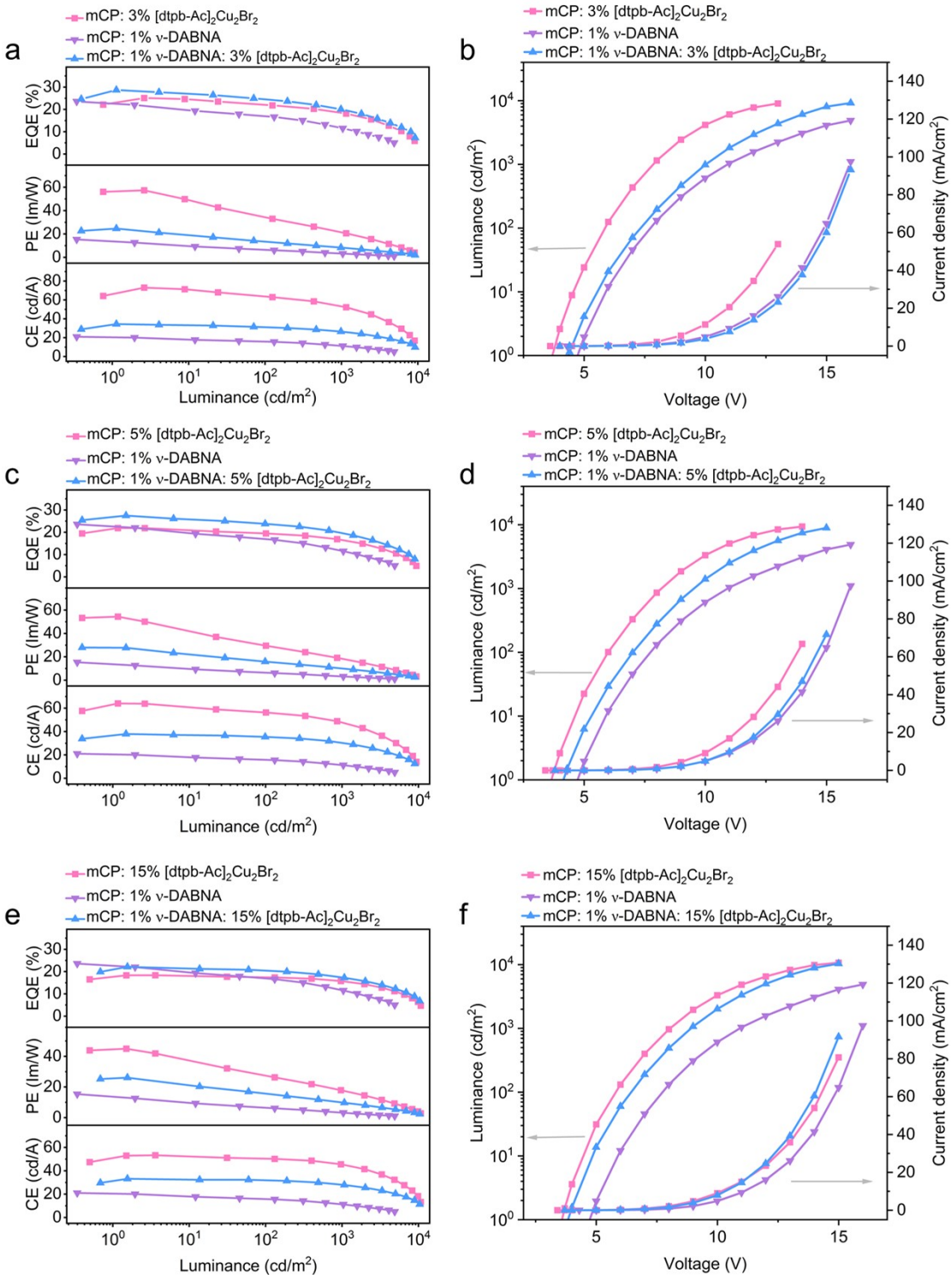

Figure S19. Device performance. a) c) e) External quantum efficiency (EQE), power efficiency (PE) and current efficiency (CE) vs luminance characteristics; b) d) f) Density−voltage−luminance characteristics.

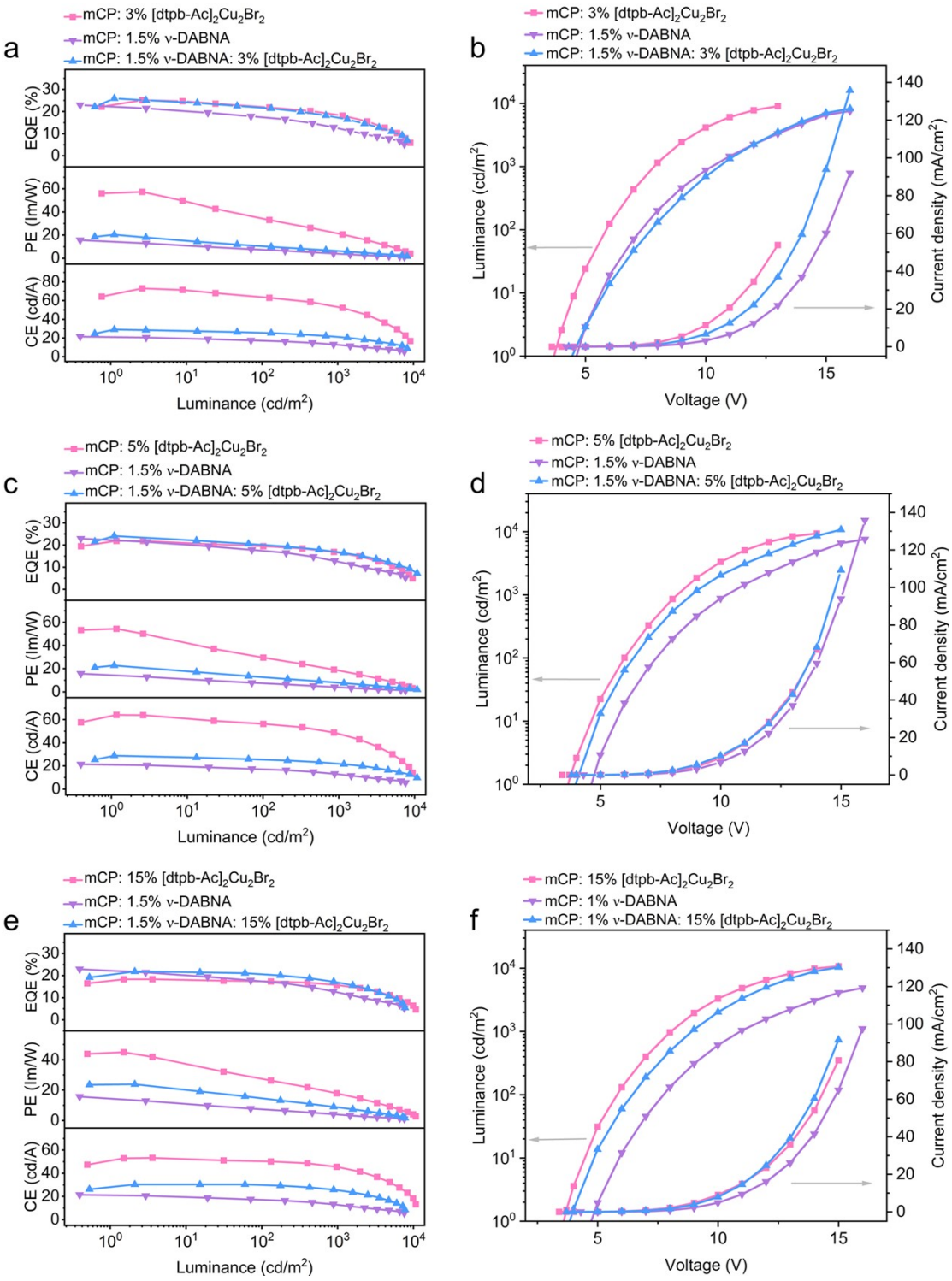

Figure S20. Device performance. a) c) e) External quantum efficiency (EQE), power efficiency (PE) and current efficiency (CE) vs luminance characteristics; b) d) f) Density−voltage−luminance characteristics.

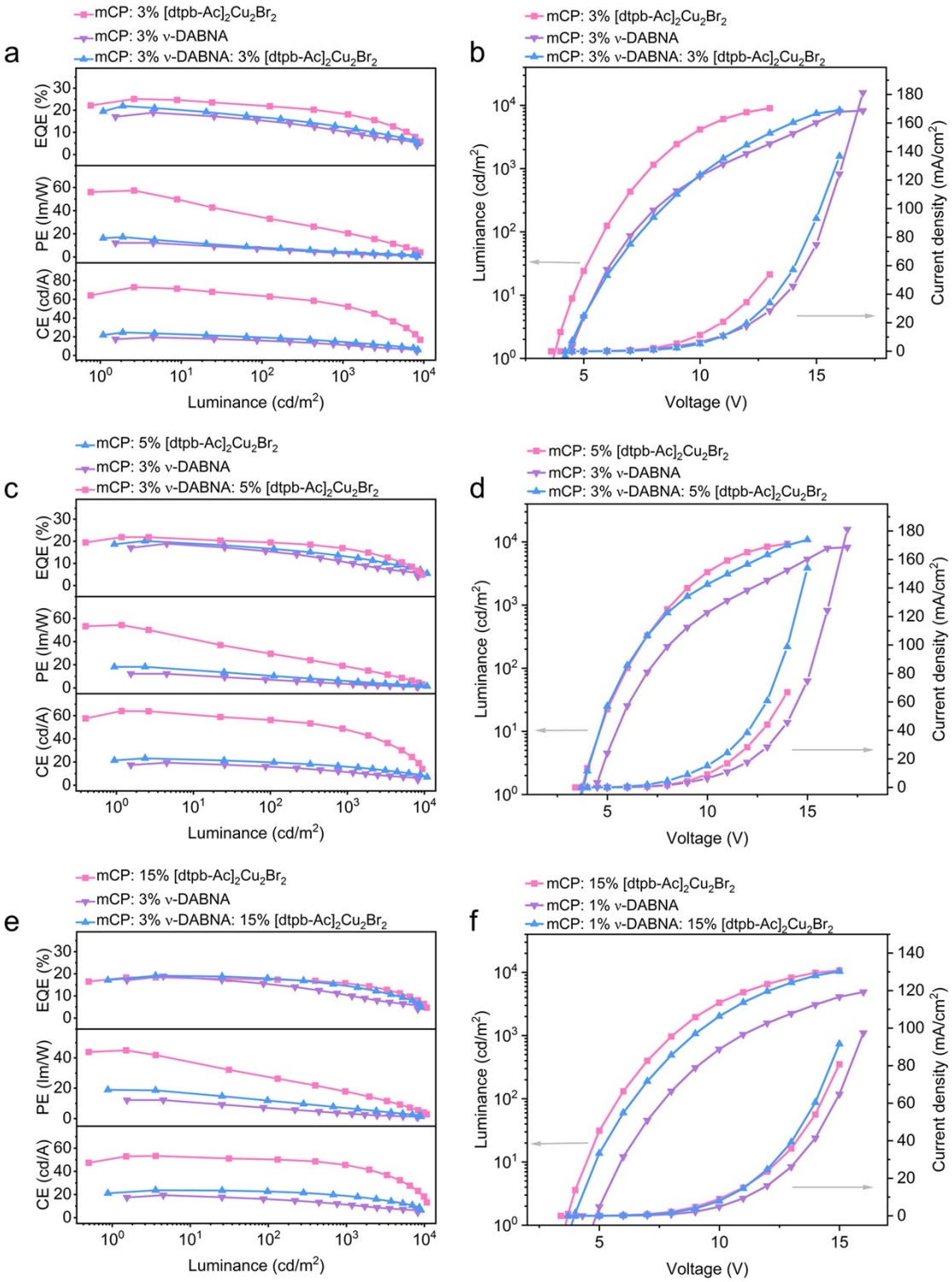

Figure S21. Device performance. a) c) e) External quantum efficiency (EQE), power efficiency (PE) and current efficiency (CE) vs luminance characteristics; b) d) f) Density−voltage−luminance characteristics.

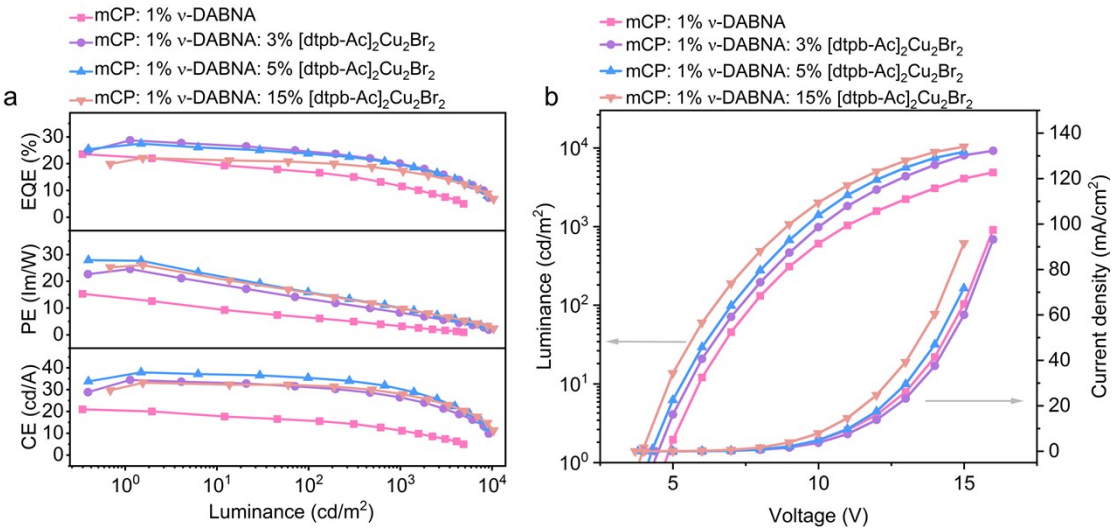

Figure S22. Device performance. a) External quantum efficiency (EQE), power efficiency (PE) and current efficiency (CE) vs luminance characteristics; b) Density−voltage−luminance characteristics.

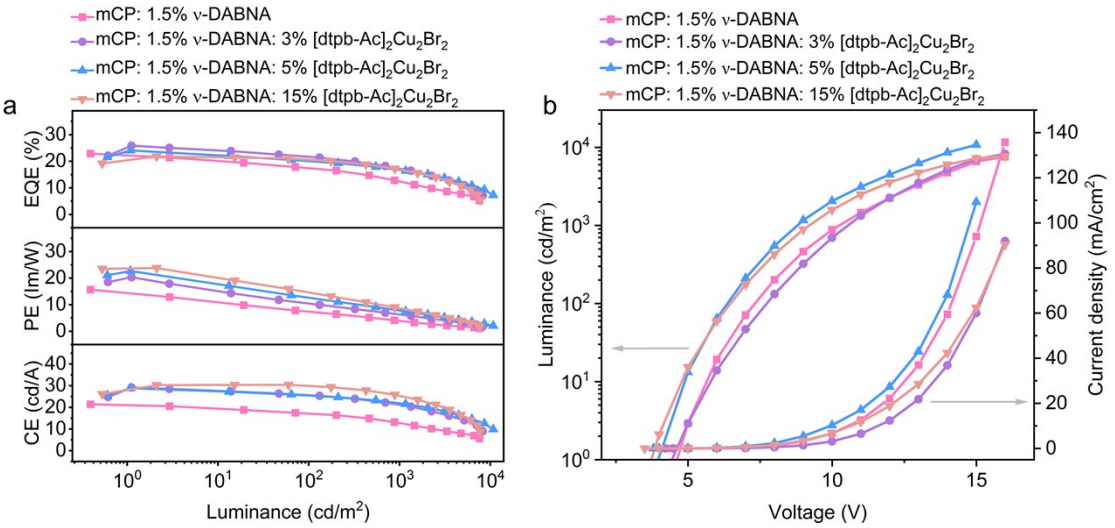

Figure S23. Device performance. a) External quantum efficiency (EQE), power efficiency (PE) and current efficiency (CE) vs luminance characteristics; b) Density−voltage−luminance characteristics.

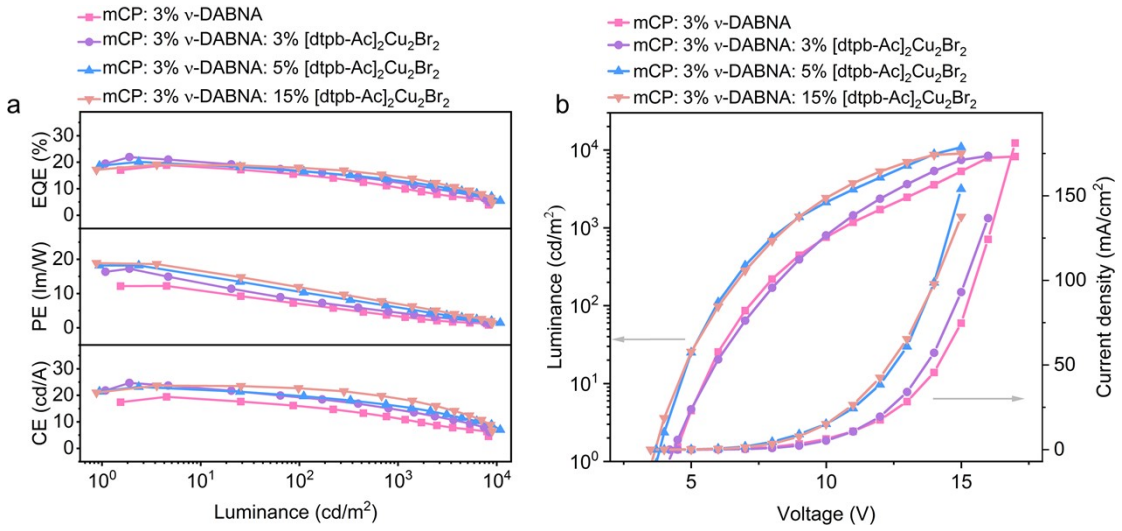

Figure S24. Device performance. a) External quantum efficiency (EQE), power efficiency (PE) and current efficiency (CE) vs luminance characteristics; b) Density−voltage−luminance characteristics.

Table S10. Summary of the device performances.

Emitter	Conc[a]	V[b]	EQE[c]	Roll-off[d]	L_{max}[e]	CE[f]	PE[g]	λ_{EL}/FWHM[h]	CIE[i]
	wt%	V	%	%	cd m^{-2}	cd A^{-1}	lm W^{-1}	nm	(x, y)
wt% *ν*-DABNA	1	4.6	22/11.7	46.9	4888	20.1	12.6	473/18.5	(0.12, 0.14)
	1.5	4.5	21.4/12.5	41.5	7576	20.6	12.9	474/18.6	(0.13, 0.15)
	3	4.4	18.9/10.5	44.5	8243	19.5	12.2	474/18.9	(0.13, 0.16)
3%[dtpb-Ac]$_2$Cu$_2$Br$_2$ wt% *ν*-DABNA	1	4.3	28.7/20	30.2	9199	34.4	24.6	473/18.7	(0.15, 0.19)
	1.5	4.4	25.9/17.4	32.9	8521	29.2	20.4	473/18.7	(0.14, 0.18)
	3	4.2	22/12.4	43.3	8415	24.7	17.2	474/18.9	(0.13, 0.18)
5%[dtpb-Ac]$_2$Cu$_2$Br$_2$ wt% *ν*-DABNA	1	4.1	27.5/19.8	27.9	8944	38	27.7	472/19	(0.17, 0.23)
	1.5	4	24.1/16.9	30.1	10780	28.9	22.7	473/18.7	(0.14, 0.19)
	3	3.7	20.2/13.2	34.7	10840	23.2	18.2	474/18.9	(0.13, 0.19)
15%[dtpb-Ac]$_2$Cu$_2$Br$_2$ wt% *ν*-DABNA	1	3.8	22.1/17.5	21.1	10370	33.2	26.1	473/19	(0.17, 0.25)
	1.5	3.6	21.8/17	22.2	7732	30.4	23.8	473/19	(0.17, 0.23)
	3	3.5	19.2/14.7	23.4	9001	23.7	18.6	474/18.9	(0.14, 0.20)

[a] Concentration of doping in mCP; [b] Turn-on voltage at 1 cd m^{-2}; [c] EQE maximum value; [d] Efficiency roll-off at 1000 cd m^{-2}; [e] Maximum luminance; [f] Maximum current efficiency; [g] Maximum power efficiency; [h] Emission wavelength and half-peak width at 1000 cd m^{-2}; [i] Commission Internatinale de L'Eclairage coordinates measured at 1000 cd m^{-2}.

Table S11. Summary of performance of previously reported representative OLEDs based on Cu(I) complexes.

Cu(I) complex as the terminal emitter		
λ_{EL}	EQE_{max}	ref
512	16.1	[7]
517	21.3	[8]
529	22.5	[9]
540	15.8	[10]
584	16.3	[11]
510	9.7	[12]
540	14.5	[13]
543	19.4	[14]
470	9	[15]
521	16.4	[16]
628	21.1	[17]
500	23.2	[18]
494	16.5	[19]
500	19.5	[20]
474	23.6	[21]
548	15.6	[22]
459	20.6	[23]
504	25.6	[24]
504	29.4	[25]
462	13	[26]
560	19.1	[27]
516	28.6	[28]
510	10.9	[29]
550	23	[30]
510	25.1	This work
Cu(I) complex as the sensitizer		
566	16.6	[31]
566	26.5	[30]
473	28.7	This work

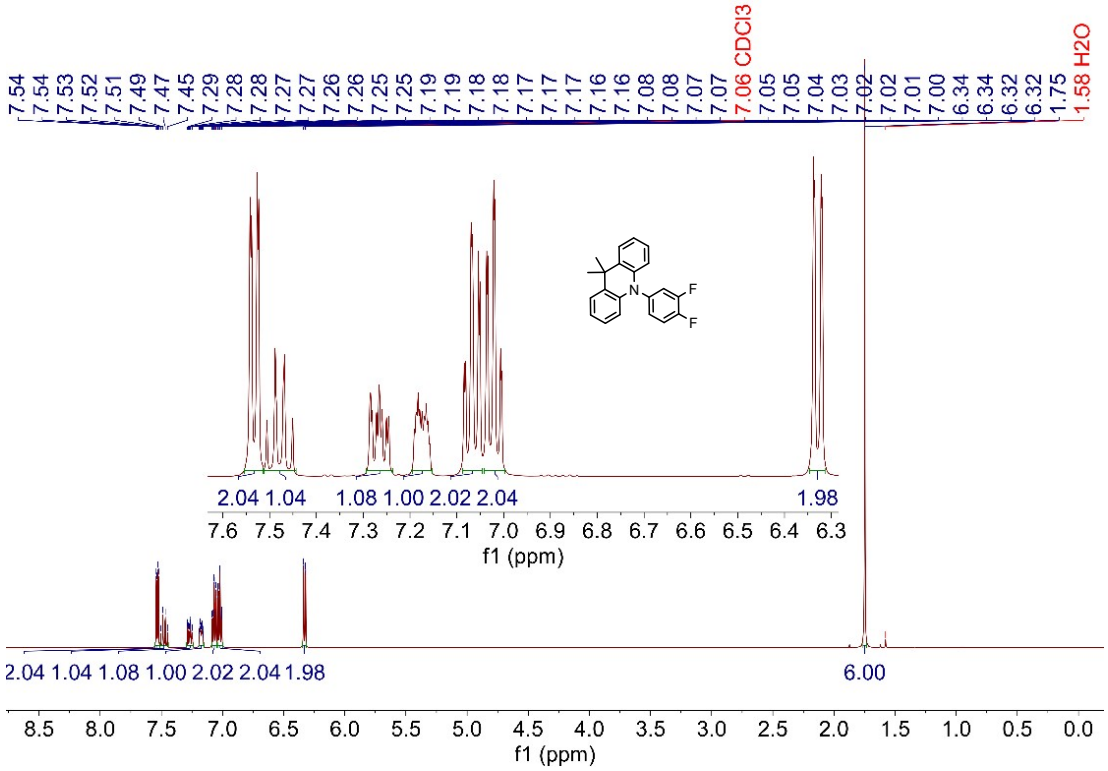

Figure S25. ^{1}H NMR spectrum of DMAC-PhF_2 in $CDCl_3$.

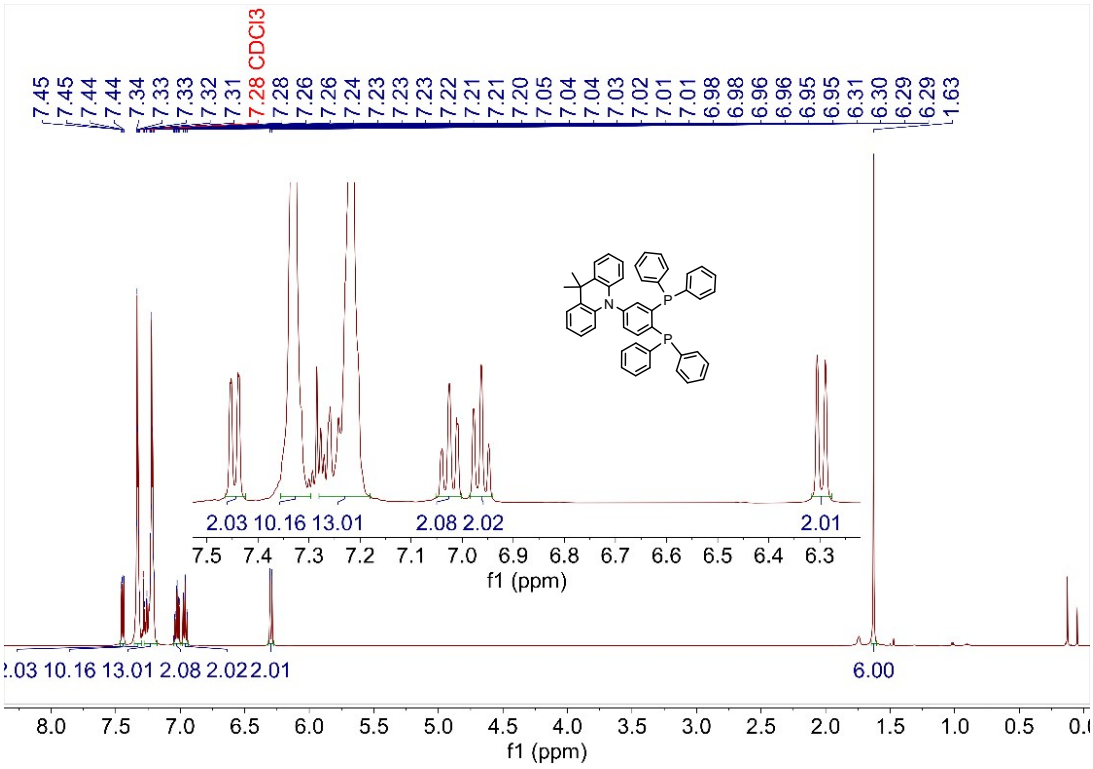

Figure S26. ^{1}H NMR spectrum of dppb-Ac in $CDCl_3$.

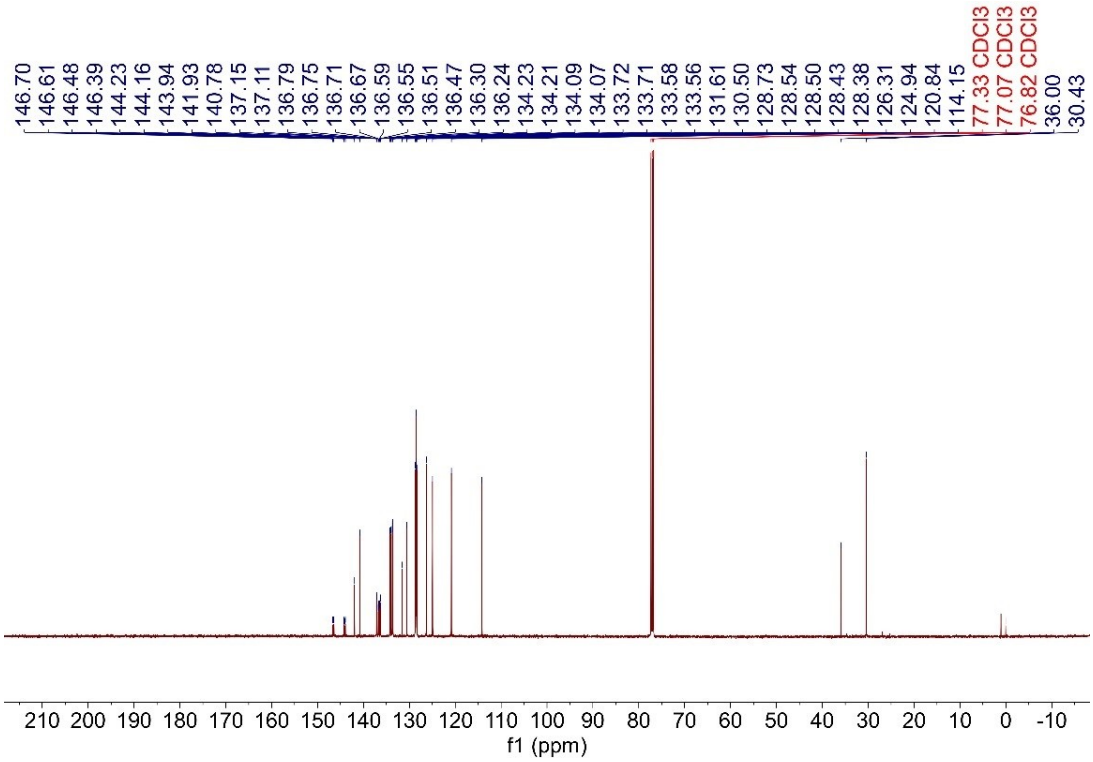

Figure S27. ^{13}C NMR spectrum of dppb-Ac in $CDCl_3$.

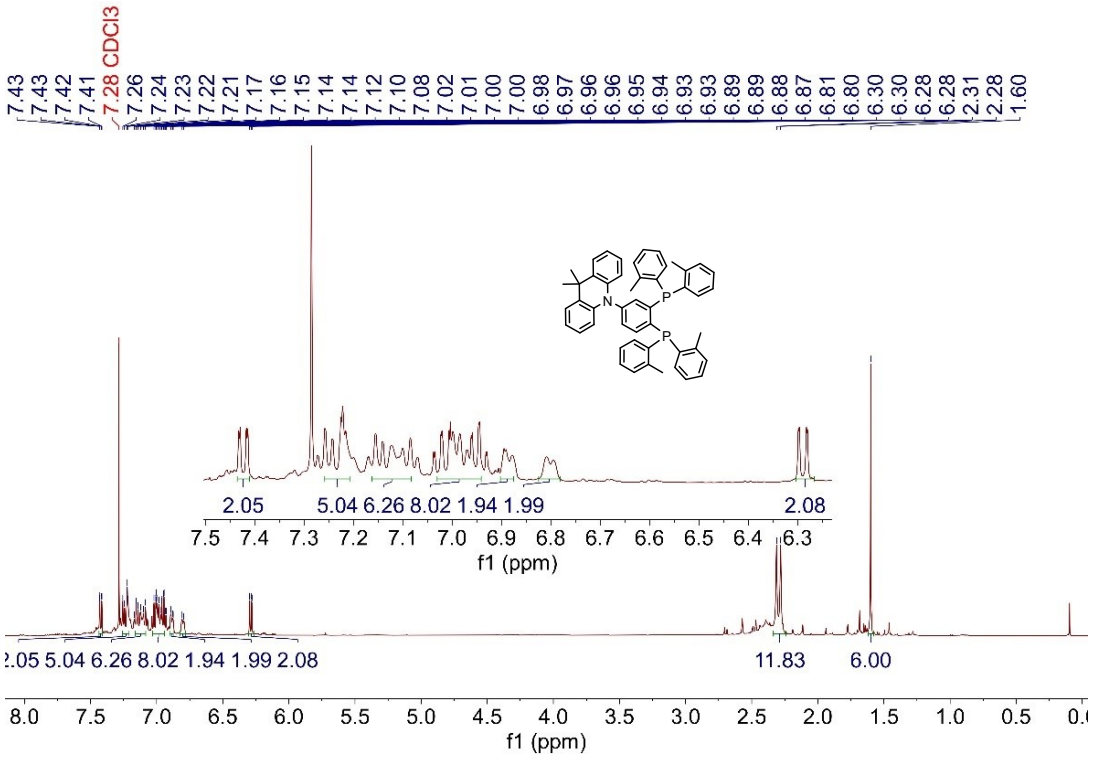

Figure S28. ^{1}H NMR spectrum of dtpb-Ac in $CDCl_3$.

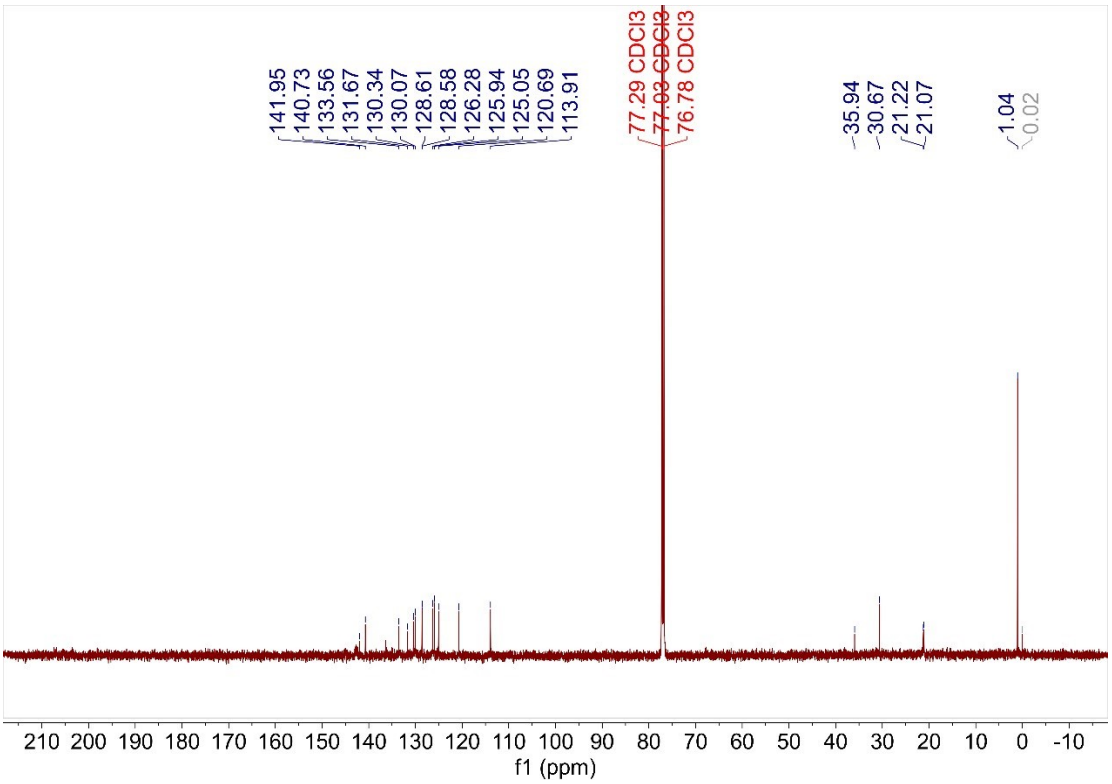

Figure S29. ^{13}C NMR spectrum of dtpb-Ac in $CDCl_3$.

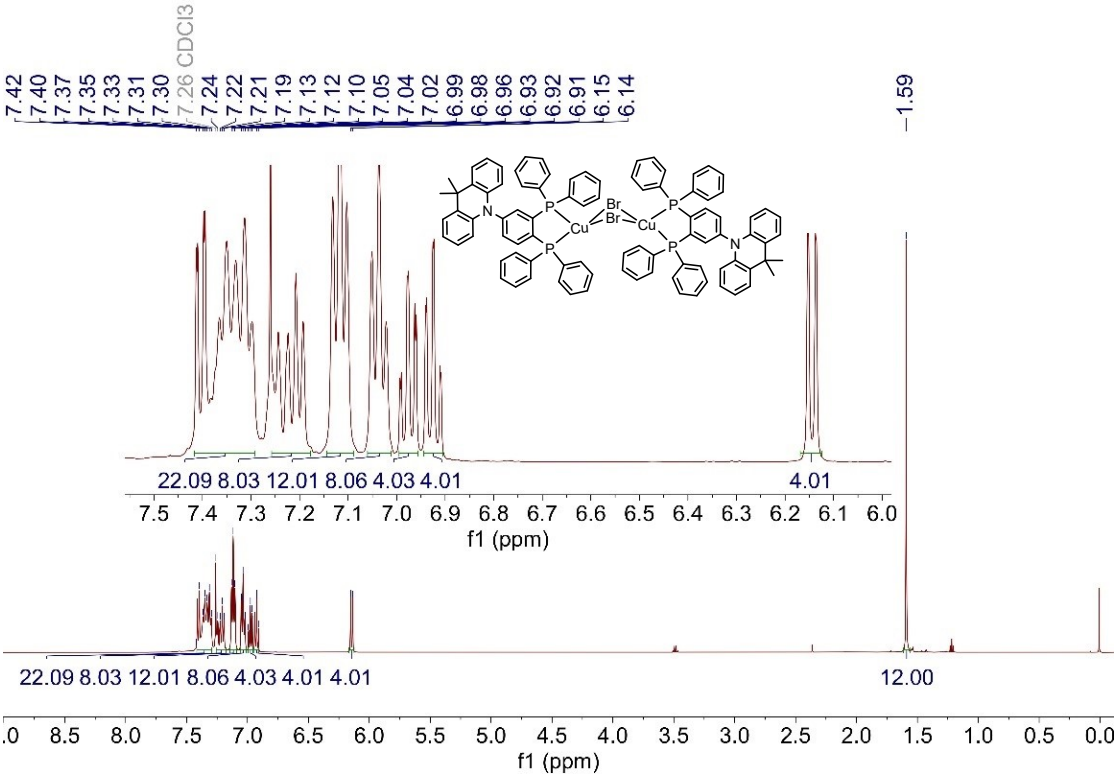

Figure S30. ^{1}H NMR spectrum of $[dppb\text{-}Ac]_2Cu_2Br_2$ in $CDCl_3$.

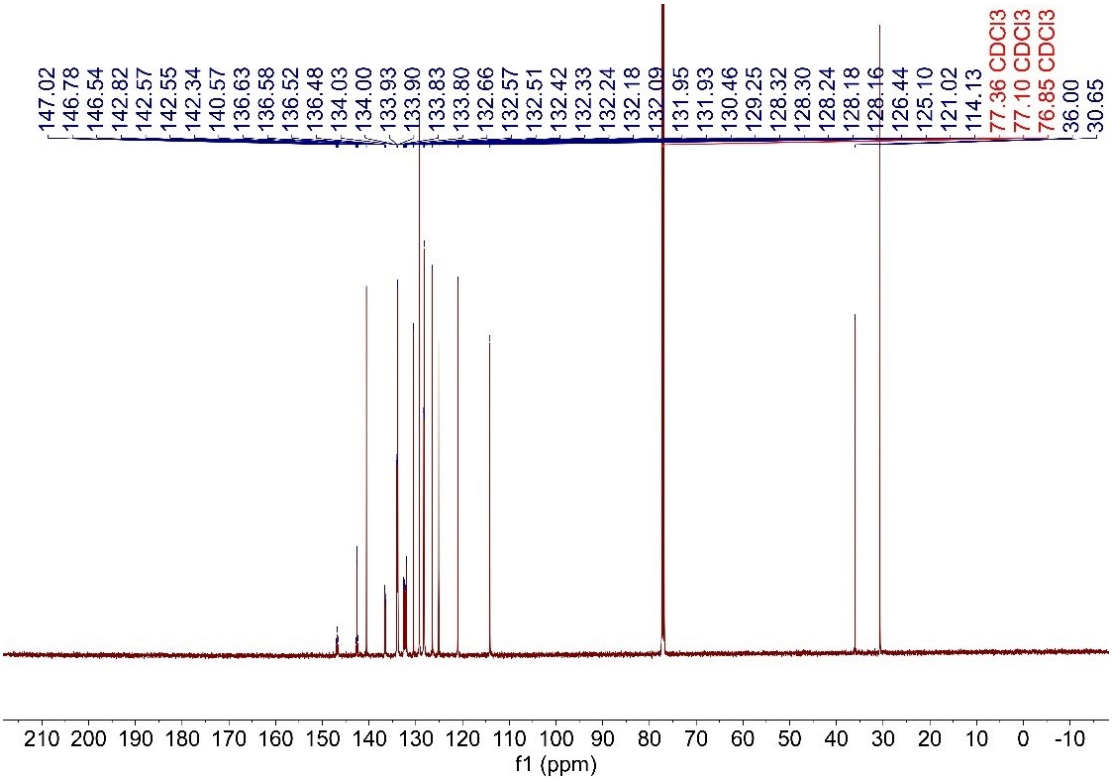

Figure S31. ^{13}C NMR spectrum of $[dppb\text{-}Ac]_2Cu_2Br_2$ in $CDCl_3$.

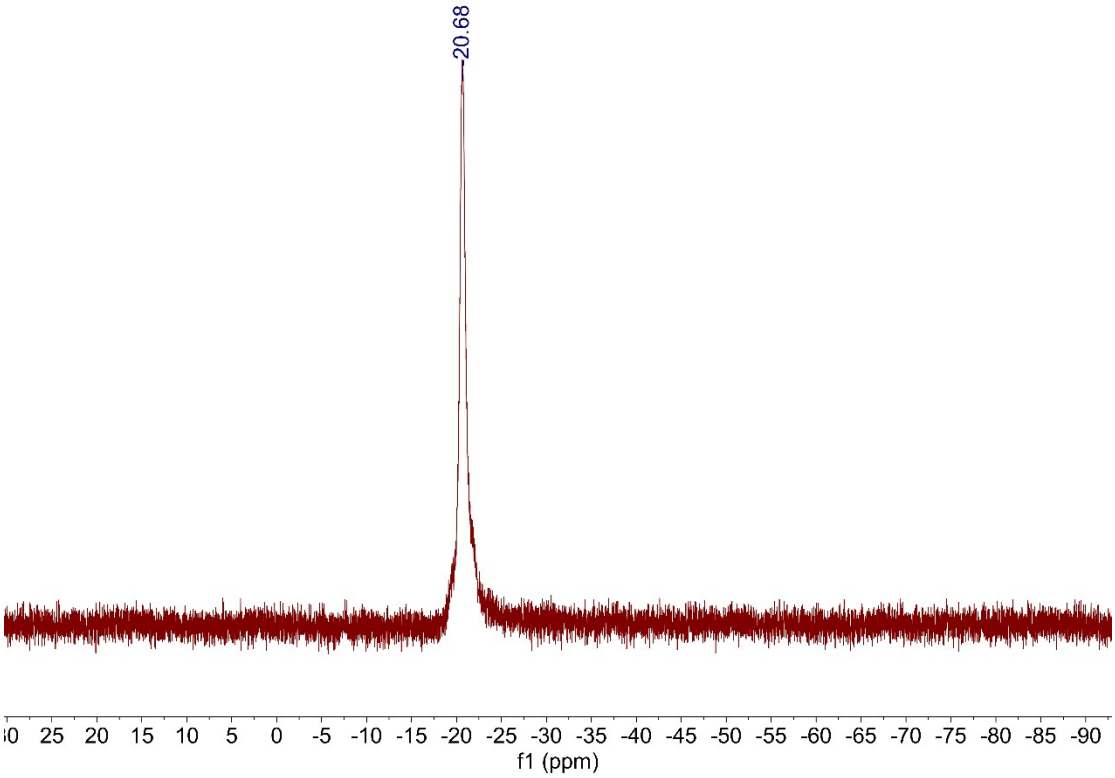

Figure S32. ^{31}P NMR spectrum of $[dppb\text{-}Ac]_2Cu_2Br_2$ in $CDCl_3$.

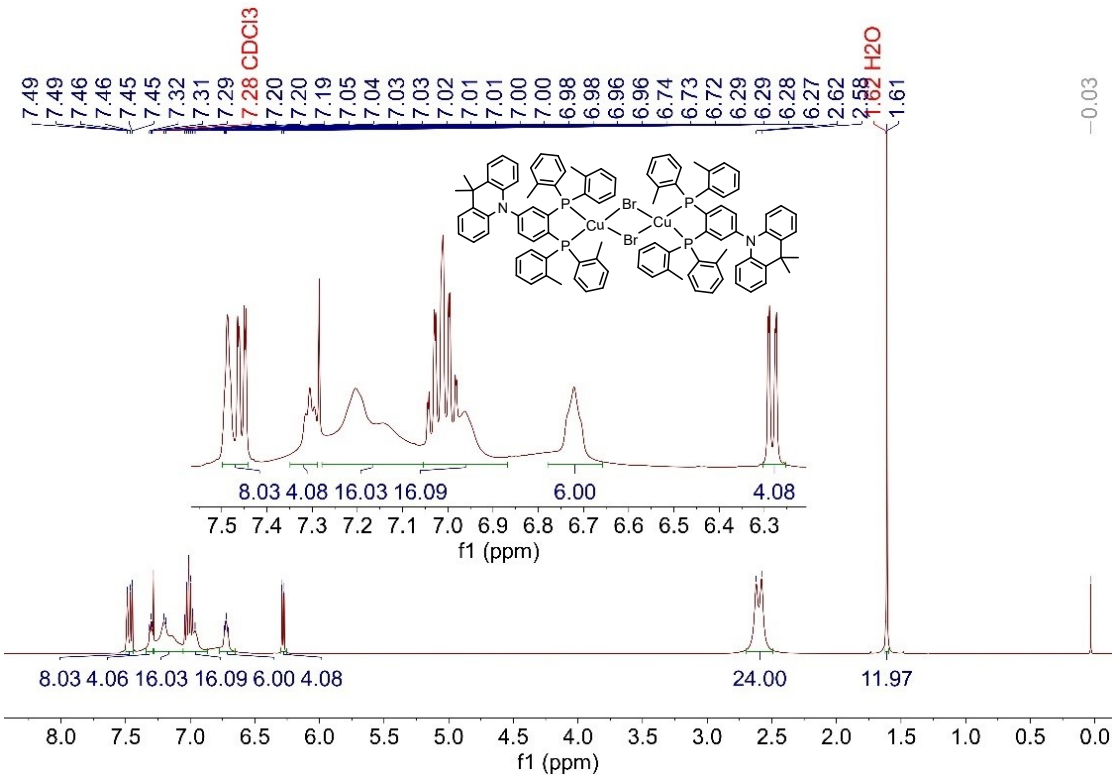

Figure S33. ^{1}H NMR spectrum of $[dtpb\text{-}Ac]_2Cu_2Br_2$ in $CDCl_3$.

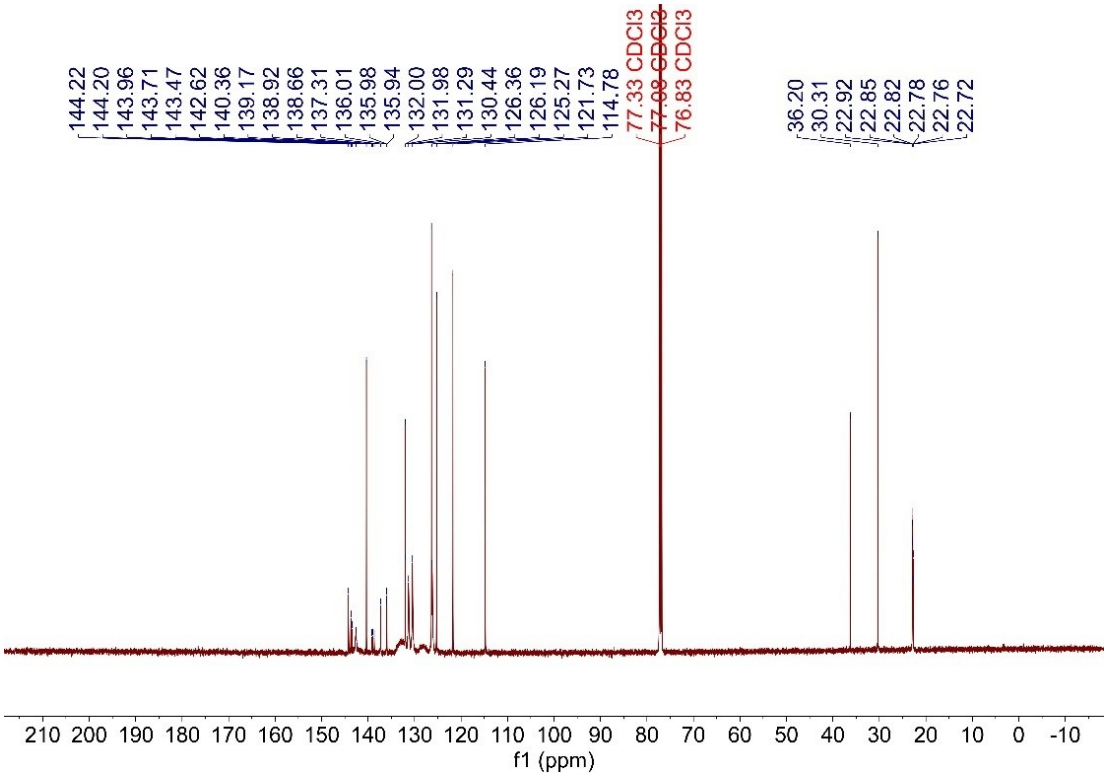

Figure S34. ^{13}C NMR spectrum of $[dtpb\text{-}Ac]_2Cu_2Br_2$ in $CDCl_3$.

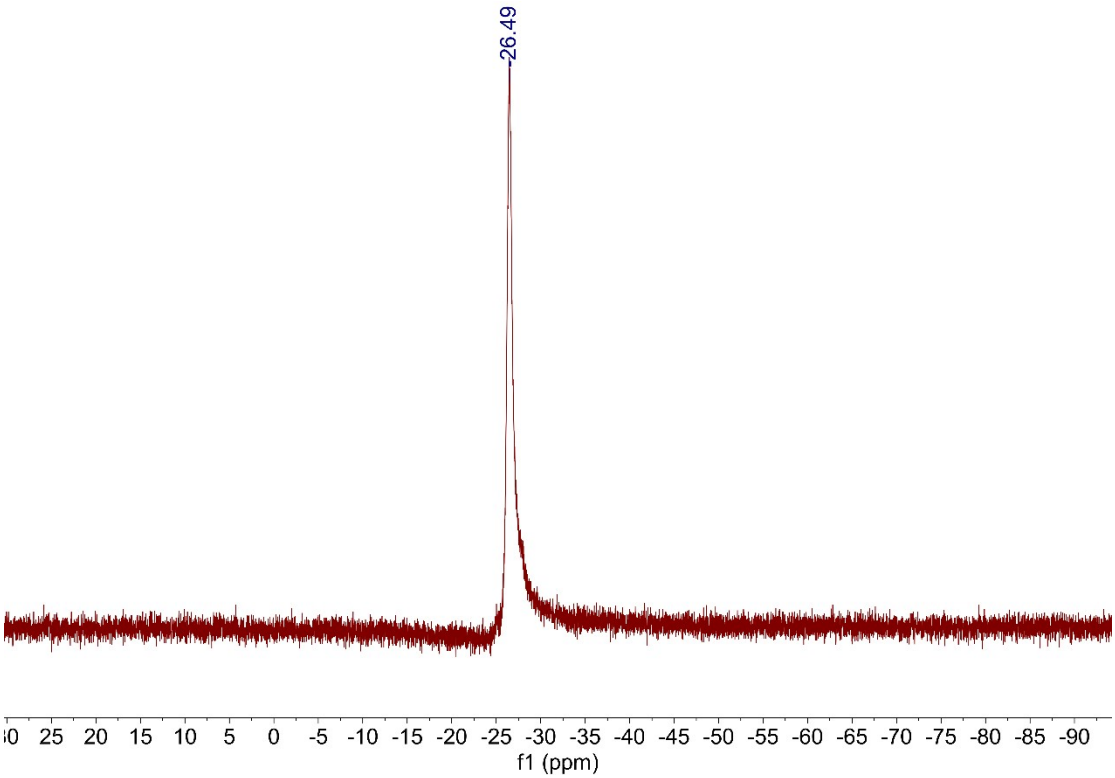

Figure S35. ^{31}P NMR spectrum of $[dtpb\text{-}Ac]_2Cu_2Br_2$ in $CDCl_3$.

Supplementary References

1. J. H. Jia, D. Liang, R. Yu, X. L. Chen, L. Meng, J. F. Chang, J. Z. Liao, M. Yang, X. N. Li, C. Z. Lu, Coordination-induced thermally activated delayed fluorescence: From non-TADF donor-acceptor-type ligand to TADF-active Ag-based complexes. *Chem. Mater.* **2019**, *32*, 620-629.

2. L. Kang, J. Chen, T. Teng, X. L. Chen, R Yu, C. Z. Lu, Experimental and theoretical studies of highly emissive dinuclear Cu(I) halide complexes with delayed fluorescence. *Dalton Trans.* **2015**, *44*, 11649-11659.
3. E. M. Espinoza, J. A. Clark, J. Soliman, J. B. Derr, M. Morales, V. I. Vullev, Practical aspects of cyclic voltammetry: How to estimate reduction potentials when irreversibility prevails. *J. Electrochem. Soc.* **2019**, *166*, H3175-H3187.
4. T. Lu, F. Chen, Multiwfn: a multifunctional wavefunction analyzer. *J. Comput. Chem.* **2012**, *33*, 580-592.
5. W. Humphrey, A. Dalke, K. Schulten, VMD: visual molecular dynamics. *J. Mol. Graph.* **1996**, *14*, 33-38.
6. Y. Y. Jing, N. Li, X. Cao, H. Wu, J. Miao, Z. Chen, M. Huang, X. Wang, Y. Hu, Y. Zou, C. Yang, Precise modulation of multiple resonance emitters toward efficient electroluminescence with pure-red gamut for high-definition displays. *Sci. Adv.*, **2023**, *9*, eadh8296.
7. J. C. Deaton, S. C. Switalski, D. Y. Kondakov, R. H. Young, T. D. Pawlik, D. J. Giesen, S. B. Harkins, A. J. M. Miller, S. F. Mickenberg, J. C. Peters, E-type delayed fluorescence of a phosphine-supported $Cu_2(\mu\text{-}NAr_2)_2$ diamond core: Harvesting singlet and triplet excitons in OLEDs. *J. Am. Chem. Soc.* **2010**, *132*, 9499–9508.
8. M. Hashimoto, S. Igawa, M. Yashima, I. Kawata, M. Hoshino, M. Osawa, Highly efficient green organic light-emitting diodes containing luminescent three-coordinate Copper(I) complexes. *J. Am. Chem. Soc.* **2011**, *133*, 10348-10351.
9. M. Osawa, M. Hoshino, M. Hashimoto, I. Kawata, S. Igawa, M. Yashima, Application of three-coordinate copper(I) complexes with halide ligands in organic light-emitting diodes that exhibit delayed fluorescence. *Dalton Trans.* **2015**, *44*, 8369-8378.
10. A. Verma, D. M. Zink, C. Fléchon, J. Leganés Carballo, H. Flügge, J. M. Navarro, T. Baumann, D. Volz, Efficient, inkjet-printed TADF-OLEDs with an ultra-soluble NHetPHOS complex. *Appl. Phys. A* **2016**, *122* 191.

11. J. Zhang, C. Duan, C. Han, H. Yang, Y. Wei, H. Xu, Balanced dual emissions from tridentate phosphine-coordinate Copper(I) complexes toward highly efficient yellow OLEDs. *Adv. Mater.* **2016**, *28*, 5975-5979.
12. D. Di, A. S. Romanov, L. Yang, J. M. Richter, J. P. H. Rivett, S. Jones, T. H. Thomas, M. A. Jalebi, R. H. Friend, M. Linnolahti, M. Bochmann, D. Credgington, High-performance light-emitting diodes based on carbene-metal-amides. *Science* **2017**, *356*, 159–163.
13. X. Li, J. Zhang, Z. Zhao, X. Yu, P. Li, Y. Yao, Z. Liu, Q. Jin, Z. Bian, Z. Lu, C. Huang, Bluish-green Cu(I) dimers chelated with thiophene ring-introduced diphosphine ligands for both singlet and triplet harvesting in OLEDs. *ACS Appl. Mater. Interfaces* **2019**, *11*, 3262-3270.
14. S. Shi, M. C. Jung, C. Coburn, A. Tadle, M. R. D. Sylvinson, P. I. Djurovich, S. R. Forrest, M. E. Thompson, Highly efficient photo-and electroluminescence from two-coordinate Cu(I) complexes featuring nonconventional n-heterocyclic carbenes. *J. Am. Chem. Soc.* **2019**, *141*, 3576-3588.
15. R. Hamze, J. L. Peltier, D. Sylvinson, M. Jung, J. Cardenas, R. Haiges, M. Soleilhavoup, R. Jazzar, P. I. Djurovich, G. Bertrand, R. E. Thompson, Eliminating nonradiative decay in Cu(I) emitters: >99% quantum efficiency and microsecond lifetime. *Science* **2019**, *363*, 601–606.
16. M. Klein, N. Rau, M. Wende, J. Sundermeyer, G. Cheng, C.-M. Che, A. Schinabeck, H. Yersin, Cu(I) and Ag(I) complexes with a new type of rigid tridentate N,P,P-ligand for thermally activated delayed fluorescence and OLEDs with high external quantum efficiency. *Chem. Mater.* **2020**, *32*, 10365-10382.
17. A. Ying, Y. H. Huang, C. H. Lu, Z. Chen, W. K. Lee, X. Zeng, T. Chen, X. Cao, C. C. Wu, S. Gong, C. Yang, High-efficiency red electroluminescence based on a carbene-Cu(I)-acridine complex. *ACS Appl. Mater. Interfaces* **2021**, *13*, 13478-13486.
18. Q. Gu, F. Chotard, J. Eng, A. M. Reponen, I. J. Vitorica-Yrezabal, A. W. Woodward, T. J. Penfold, D. Credgington, M. Bochmann, A. S. Romanov, Excited-state lifetime modulation by twisted and tilted molecular design in carbene-metal-amide photoemitters. *Chem. Mater.* **2022**, *34*, 7526-7542.

19. A. Ruduss, B. Turovska, S. Belyakov, K. A. Stucere, A. Vembris, G. Baryshnikov, H. Agren, J. C. Lu, W. H. Lin, C. H. Chang, K. Traskovskis, Thiazoline carbene-Cu(I)-amide complexes: Efficient white electroluminescence from combined monomer and excimer emission. *ACS Appl. Mater. Interfaces* **2022**, *14*, 15478-15493.
20. N. Zhang, H. Hu, L. Qu, R. Huo, J. Zhang, C. Duan, Y. Meng, C. Han, H. Xu, Overcoming efficiency limitation of cluster light-emitting diodes with asymmetrically functionalized biphosphine Cu_4I_4 cubes. *J. Am. Chem. Soc.* **2022**, *144*, 6551-6557.
21. R. Tang, S. Xu, T. L. Lam, G. Cheng, L. Du, Q. Wan, J. Yang, F. F. Hung, K. H. Low, D. L. Phillips, C. M. Che, Highly robust Cu(I)-TADF emitters for vacuum-deposited OLEDs with luminance up to 222200 cd m^{-2} and device lifetimes (LT_{90}) up to 1300 hours at an initial luminance of 1000 cd m^{-2}. *Angew. Chem. Int. Ed.* **2022**, *61*, e202203982.
22. Y. Li, S. Xu, X. Zhang, Y. Man, J. Zhang, G. Zhang, S. Chen, C. Duan, C. Han, H. Xu, Bulk passivation enables hundredfold-enhanced electroluminescence of monophosphine Cu_4I_4 cubes. *Angew. Chem. Int. Ed.* **2023**, *62*, e202308410.
23. H. J. Wang, Y. Liu, B. Yu, S. Q. Song, Y. X. Zheng, K. Liu, P. Chen, H. Wang, J. Jiang, T. Y. Li, A configurationally confined thermally activated delayed fluorescent two-coordinate Cu(I) complex for efficient blue electroluminescence. *Angew. Chem. Int. Ed.* **2023**, *62*, e202217195.
24. N. Zhang, L. Qu, S. Dai, G. Xie, C. Han, J. Zhang, R. Huo, H. Hu, Q. Chen, W. Huang, H. Xu, Intramolecular charge transfer enables highly-efficient X-ray luminescence in cluster scintillators. *Nat. Commun.* **2023**, *14*, 2901.
25. N. Zhang, Y. Li, S. Han, Y. Wei, H. Hu, R. Huo, C. Duan, J. Zhang, C. Han, G. Xie, H. Xu, Cluster light-emitting diodes containing copper iodine cube with 100 % exciton utilization using host-cluster synergy. *Angew. Chem. Int.* **2023**, *62*, e202305018.
26. R. Li, A. Ying, Y. Tan, Y. Ai, S. Gong, Efficient blue photo- and electroluminescence from CF3-Decorated Cu(I) complexes. *Chem. Eur. J.* **2024**, *30*, e202400817.

27. J.-J. Wang, L.-Z. Feng, G. Shi, J.-N. Yang, Y.-D. Zhang, H. Xu, K.-H. Song, T. Chen, G. Zhang, X.-S. Zheng, F. Fan, Z. Xiao, H.-B. Yao, High efficiency warm-white light-emitting diodes based on copper–iodide clusters. *Nat. Photon.* **2023**, *18*, 200-206.
28. A. Ying, Y. Tan, S. Gong, Highly efficient copper(I) emitters supported by secondary metal-ligand interactions. *Adv. Opt. Mater.* **2024**, *12*, 230333.
29. Y. Tan, A. Ying, Y. Liu, X. Cai, L. Zhan, Z. Bin, J. You, C. Li, S. Gong, Copper(I) TADF exciplexes via metal-perturbed through-space charge transfer for efficient OLEDs. *Chem. Eng. J.*, **2024**, *487*, 150618.
30. D. Volz, Y. Chen, M. Wallesch, R. Liu, C. Flechon, D. M. Zink, J. Friedrichs, H. Flugge, R. Steininger, J. Gottlicher, C. Heske, L. Weinhardt, S. Brase, F. So, T. Baumann, Bridging the efficiency gap: Fully bridged dinuclear Cu(I)-complexes for singlet harvesting in high-efficiency OLEDs. *Adv. Mater.* **2015**, *27*, 2538-2543.
31. L. Zhan, A. Ying, Y. Qi, K. Wu, Y. Tang, Y. Tan, Y. Zou, G. Xie, S. Gong, C. Yang, Copper(I) complex as sensitizer enables high-performance organic light-emitting diodes with very low efficiency roll-off. *Adv. Funct. Mater.* **2021**, *31*, 2106345.